AD-A168 106 EFFECT OF TIME-TEMPERATURE PATH OF CURE ON THE WATER ABSORPTION OF HIGH T..(U) PRINCETON UNIV NJ DEPT OF CHEMICAL ENGINEERING M T ARONHIME ET AL. MAY 86 TR-8 1/1

UNCLASSIFIED N00014-84-K-0021 F/G 11/9 NL

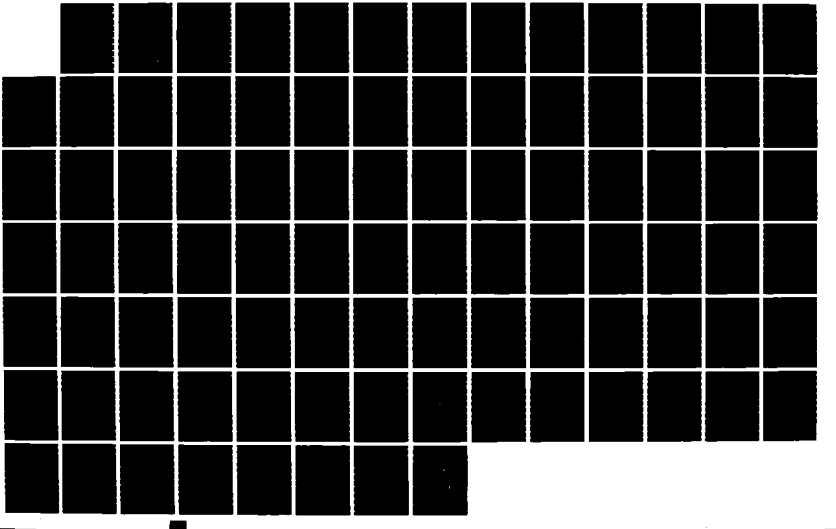

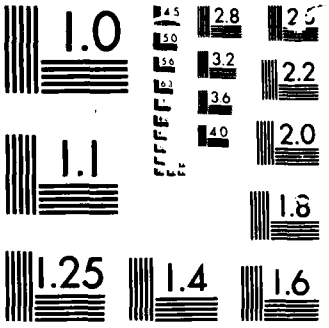

MICROCOPY CHART

OFFICE OF NAVAL RESEARCH

Contract N00014-84-K-0021

TECHNICAL REPORT NO. 8

EFFECT OF TIME-TEMPERATURE PATH OF CURE ON THE WATER ABSORPTION OF HIGH T_g EPOXY RESINS

by

M. T. Aronhime and John K. Gillham

for publication in

Journal of Applied Polymer Science

PRINCETON UNIVERSITY
Polymer Materials Program
Department of Chemical Engineering
Princeton, New Jersey 08544

May 1986

Principal Investigator
John K. Gillham
(609) 452-4694

SECURITY CLASSIFICATION OF THIS PAGE (When Data Entered)

REPORT DOCUMENTATION PAGE		READ INSTRUCTIONS BEFORE COMPLETING FORM
1 REPORT NUMBER Technical Report No. 8	2 GOVT ACCESSION NO N/A	3 RECIPIENT'S CATALOG NUMBER N/A
4 TITLE (and Subtitle) Effect of Time-Temperature Path of Cure on the Water Absorption of High T_g Epoxy Resins		5 TYPE OF REPORT & PERIOD COVERED 7/1/84 - 5/1/86 6 PERFORMING ORG REPORT NUMBER
7 AUTHOR(s) M. T. Aronhime and John K. Gillham		8 CONTRACT OR GRANT NUMBER(s) N00014-84-K-0021
9 PERFORMING ORGANIZATION NAME AND ADDRESS Polymer Materials Program Department of Chemical Engineering Princeton University, Princeton, NJ 08544		10 PROGRAM ELEMENT, PROJECT, TASK AREA & WORK UNIT NUMBERS
11 CONTROLLING OFFICE NAME AND ADDRESS Office of Naval Research 800 North Quincy Street Arlington, VA 22217		12 REPORT DATE May 1986 13 NUMBER OF PAGES 84
14 MONITORING AGENCY NAME & ADDRESS (if different from Controlling Office)		15 SECURITY CLASS (of this report) Unclassified 15a DECLASSIFICATION DOWNGRADING SCHEDULE

16 DISTRIBUTION STATEMENT (of this Report)

Approved for public release; distribution unlmmited

17 DISTRIBUTION STATEMENT (of the abstract entered in Block 20, if different from Report)

NA

18 SUPPLEMENTARY NOTES

The view, opinions, and/or findings contained in this report are those of the author(s) and should not be construed as an official Department of the Navy position, policy, or decision, unless so designated by other documentation.

19 KEY WORDS (Continue on reverse side if necessary and identify by block number)

Water Absorption
Epoxies
Effect of Cure
Effect of Structure
Equilibrium Absorption
Transient Absorption

20 ABSTRACT (Continue on reverse side if necessary and identify by block number)

The effect of different time-temperature paths of cure on the water absorption of high T_g epoxy resins has been investigated. The resins were cured isothermally at elevated temperatures for different times, with the following results: as extent of cure increased, the glass transition temperature (T_g) increased, the room temperature (RT) modulus decreased, the RT density decreased, the RT diffusion coefficient appeared to decrease, and the RT equilibrium absorption of water increased. The decrease in RT density is

DD FORM 1 JAN 73 1473 EDITION OF 1 NOV 65 IS OBSOLETE
S/N 0102-LF-014-6601

SECURITY CLASSIFICATION OF THIS PAGE (When Data Entered)

related to an increase in volume, which controls the amount of water absorbed. A qualitative model accounts for the increase in RT volume with increasing cure. The model is based on a restricted decrease of free volume on cure due to the rigid molecular segments in the cured resin systems. The sorption isotherms can be characterized by the dual mode theory at low activities but at high activities the sorption is complicated by penetrant clustering. A thermodynamic approach, independent of the absorption model, can correlate sorption data at different temperatures. The diglycidyl resin was also cured for extended times at three temperatures in an effort to achieve full cure at each temperature. For these, the higher the cure temperature the lower the RT density, which could result from the lower initial density of materials cured at higher temperatures. Their equilibrium water absorption increased with increasing cure temperature, consistent with the decrease in RT density. The systems studied were a diglycidyl ether of bisphenol A cured with an aromatic tetrafunctional diamine, trimethylene glycol di-p-aminobenzoate ($T_{g\infty}$ = 156°C), and a triglycidyl ether of tris(hydroxyphenyl)methane cured with the same amine ($T_{g\infty}$ = 268°C).

T subgirtinity

Effect of Time-Temperature Path of Cure

On the Water Absorption of High T_g Epoxy Resins

M. T. Aronhime, X. Peng and J. K. Gillham
Department of Chemical Engineering
Polymer Materials Program
Princeton University
Princeton, New Jersey 08544

and

R. D. Small
Engineering Research Center
AT&T Technologies
P.O. Box 900
Princeton, New Jersey 08540

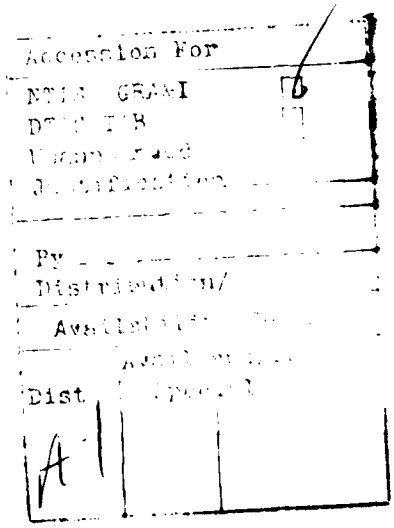

ABSTRACT

The effect of different time-temperature paths of cure on the water absorption of high T_g epoxy resins has been investigated. The resins were cured isothermally at elevated temperatures for different times, with the following results: as extent of cure increased, the glass transition temperature (T_g) increased, the room temperature (RT) modulus decreased, the RT density decreased, the RT diffusion coefficient appeared to decrease, and the RT equilibrium absorption of water increased. The decrease in RT density is related to an increase in volume, which controls the amount of water absorbed. A qualitative model accounts for the increase in RT volume with increasing cure. The model is based on a restricted decrease of free volume on cure due to the rigid molecular segments in the cured resin systems. The sorption isotherms can be characterized by the dual mode theory at low activities but at high activities the sorption is complicated by penetrant clustering. A thermodynamic approach, independent of the absorption model, can correlate sorption data at different temperatures. The diglycidyl resin was also cured for extended times at three temperatures in an effort to achieve full cure at each temperature. For these, the higher the cure temperature the lower the RT density, which could result from the lower initial density of materials cured at higher temperatures. Their equilibrium water absorption increased with increasing cure temperature, consistent with the decrease in RT density. The systems studied were a diglycidyl ether of bisphenol A cured with an aromatic tetrafunctional diamine, trimethylene glycol di-p-aminobenzoate ($T_{g\infty}$ = 156°C), and a triglycidyl ether of tris(hydroxyphenyl)methane cured with the same amine ($T_{g\infty}$ = 268°C).

INTRODUCTION

Epoxy resins play an important role in the aerospace and electronics industries. The effect of the environment is critical, because water vapor absorbed from the surroundings affects mechanical (1,2) and electrical properties (3,4), usually in a harmful manner. It is therefore important to understand the factors that control water absorption in cured epoxy resins.

Two factors influential in the moisture absorption behavior of cured epoxy resins are the presence of appropriately sized holes and the nature of the polymer-water affinity (5). Our laboratory has been concerned for several years with the effect of cure on water absorption in epoxies. It has been observed that the cure process is important in determining the amount of space in the cured matrix available for water sorption (6-9), whereas the initial selection of epoxy and curing agent may be more influential in determining polymer-water affinity (8).

It was observed (7) that post-curing an epoxy resin yielded an interesting result (Fig. 1): the glass transition temperature (T_g) increased on post-cure, but the room temperature (RT) shear modulus of the more highly cured material was lower than the RT modulus of the undercured resin. A similar observation was made in another study, where higher temperatures of post-cure yielded lower tensile moduli at RT (10). These results were anomalous since higher post-cure temperatures were expected to increase the crosslinking and hence the stiffness.

Since a lower glassy state modulus implied a lower density, studies were undertaken to investigate the effect of extent of cure on RT density and water

absorption (water absorption was considered to be intimately related to the density of the material) (6-9). These studies, focusing on different high T_g epoxy/amine systems, all yielded the same results: as extent of cure increased, T_g increased, RT density decreased, and RT water absorption increased. Thus, T_g and RT density were found to be inversely related. The inverse T_g vs. RT density relationship had been reported earlier for six epoxy/anhydride systems (11).

The decrease in RT modulus (or density) with an increase in T_g appears to be a somewhat general phenomenon, and one not limited to thermosets. Examination of the data of Ueberreiter and Kanig (12) on pure polystyrene fractions reveals that the extrapolated glassy-state specific volume at absolute zero increased (density decreased) as molecular weight (and hence T_g) increased. Also, for poly(methyl methacrylate) (PMMA), the T_g of syndiotactic PMMA is greater than the T_g of isotactic PMMA, but the density and modulus of isotactic PMMA at 30°C are greater than the corresponding quantities for the syndiotactic form (13). Several additional studies on different epoxy/amine systems report modulus-temperature data, and in most cases the RT modulus decreases as T_g increases (14-17). In these studies, T_g increased because of different concentrations of curing agent (14), different epoxy monomers cured with the same amine (15), and decreasing amounts of an antiplasticizer added to the epoxy/amine formulation (16,17). An antiplasticizer is a chemical defined by its ability to increase the modulus of the cured product, in contrast to the effect expected from the addition of a plasticizer. However, in the reports cited, the antiplasticizer behaved like a plasticizer with

respect to causing a decrease in the T_g of the cured product. Boyer (18) cited several studies on the styrene-divinyl benzene system, where increasing concentrations of divinyl benzene led to lower RT densities. The normal shrinkage on polymerization was thus inhibited by the crosslinks, resulting in a lower RT density (18).

In the previous work from this laboratory, the extent of cure was changed by curing isothermally for different times. Curing isothermally was considered to give most control over the curing process. Different temperatures of cure can be expected to give rise to different materials because of the different activation energies of the competing reactions (19) and the dependence of the initial densities on the cure temperature.

In the present work, the effect of time-temperature path of cure on the RT sorption behavior and density of di- and trifunctional epoxy resins cured with the same tetrafunctional amine was investigated. Throughout this work, "difunctional system" means the system consisting of the difunctional epoxy cured with the tetrafunctional amine; "trifunctional system" refers to the system consisting of the trifunctional epoxy cured with the tetrafunctional amine. The difunctional system had a lower maximum glass transition temperature ($T_{g\infty}$ = 156°C) than the different difunctional materials studied previously (6-8); a wider temperature range between full cure and thermal degradation was thus possible. The effect of extent of cure on the equilibrium moisture gains and models for the equilibrium and transient sorption were examined. Finally, a qualitative model is discussed to aid in the understanding of the anomalous T_g versus RT density relationship.

Representative data are presented and discussed here; a more complete report is available (20).

EXPERIMENTAL

1. Materials

The resin systems studied (Fig. 2) were a diglycidyl ether of bisphenol A (DER 337, Dow Chemical Co.) cured with a stoichiometric amount of trimethylene glycol di-p-aminobenzoate ("TMAB", Polacure 740M, Polaroid Co.), and a triglycidyl ether of tris(hydroxy phenyl)methane (XD 7342.00, Dow Chemical Co.) cured with a stoichiometric amount of TMAB. Isothermal time-temperature-transformation (TTT) cure diagrams are shown (Figs. 3a and 3b). $T_{g\infty}$ for DER337/TMAB is about 156°C (0.7 Hz), and $T_{g\infty}$ for XD7342/TMAB is about 268°C (0.5 Hz). TTT diagrams are constructed by plotting cure temperature versus the times to gelation and vitrification, as determined by torsional braid analysis, for a series of isothermal cures (21). After prolonged isothermal cure, the resins are cooled to -170°C, post-cured to 240°C (DER337/TMAB) or 280°C (XD7342/TMAB), and then cooled again to -170°C, all temperature scans being conducted at 1.5°C/min. The scan from -170°C to the post-cure temperature yields the T_g after cure, whereas the scan from the post-cure temperature to -170°C yields a transition temperature denoted here as $T_{g\infty}'$. An average of these values of $T_{g\infty}'$ from a series of isothermal runs is taken as an operational value of $T_{g\infty}$. Details on the construction and interpretation of these diagrams have been published (21). The TTT diagrams are useful for determining the time required at a given temperature to reach a given region

of matter (i.e., liquid region, sol/gel rubber region, or glassy regions) or a given relative degree of cure.

The epoxide equivalent weight (EEW) of DER 337 is in the range 230-280 gm/equivalent (22). A value was determined for the sample used following a procedure described in the literature (23); an average of two trials yielded an EEW of 246.1. The EEW of XD7342 (162) and the equivalent weight of TMAB (78.5) were provided by the manufacturers.

2. Cure Procedure

a. Difunctional System

DER 337 is a highly viscous material at RT, and TMAB is a crystalline powder with a melting point of 125°C. Solid TMAB was added to epoxy which had been heated to 125°C. The mixture was stirred for three minutes and then the homogeneous material was poured into aluminum weighing dishes and stored in a desiccator at 0°C (T_{go} = 5°C, where T_{go} is the glass transition temperature of the uncured reactants).

The time-temperature path of cure was varied in two ways: curing isothermally for different times; and curing at three different temperatures for extended periods of time in an effort to achieve full cure. For the former case, specimens were cured at 161°C for 3, 5, 11, 29, 72, and 341 hr., followed by cooling slowly to RT (~1°C/min). The isothermal cure temperature of 161°C was selected because a wide range of extents of cure could be conveniently studied, from low to high degrees of cure. For the latter case, the cure conditions were 131°C/168 hr., 145°C/96 hr., and 166°C/72 hr., followed by cooling slowly to RT.

The basic cure procedure was the same for all specimens: remove desiccator containing the mixed reactants from cold storage and allow to come to RT; degas material in aluminum weighing dishes at 100°C for 20 min.; fill preheated (100°C) aluminum foil-lined casting molds (5.85 cm. x 1.25 cm. x ~0.1 cm.) with approximately the same weight of material; degas material in molds at 100°C for 10 min.; place molds in an oven which has been preheated to the cure temperature, and cure for specified time; cool slowly to RT. Cure time was measured from the time the specimens were placed in the oven. All cures were performed in an inert (N_2) atmosphere. Aluminum foil-lined casting molds were used in order to eliminate the need to use release agent; the aluminum foil could be easily peeled from the cured specimens.

b. Trifunctional System

Solid TMAB was added to liquid XD7342 which had been heated to 135°C. The mixture was stirred for eight minutes, and then transferred to aluminum weighing dishes and stored in a desiccator at 4°C (T_{go} = 18°C).

This system was cured isothermally at 195°C for 0.25, 0.5, 5, 24, 96, and 240 hr., followed by free cooling to RT. The temperature of 195°C was selected as a compromise between the desire to obtain full cure after a long isothermal cure and the necessity to avoid degradation. However, even 240 hr. at 195°C was probably not sufficient to obtain full cure (see RESULTS section).

The cure procedure paralleled that for the difunctional system, except each degassing (before and after mold filling) was for 30 min. All cures were performed in an inert (N_2) atmosphere.

3. Water Absorption and Density Measurements

In order to study water absorption, the cured specimens were suspended above aqueous salt solutions in rubber-stoppered test tubes; the test tubes had been previously equilibrated in a constant temperature water bath (24.5±0.1°C). Each test tube contained one specimen. Seven relative humidities (RH) were used (Table I). Two specimens from each cure condition were employed at each RH. For the XD7342/TMAB system, absorption experiments were also performed at 35.0±0.1°C for the six extents of cure at 195°C and at 45.0±0.1°C for one extent of cure (24 hr.).

After the cured specimens had been removed from the oven, a high-speed drill was used to make small holes in the specimens, so that they could be suspended from stainless steel wires over the saturated solutions. Prior to insertion in the test tubes, the specimens were held at 100°C under vacuum for 12 hr., followed by free cooling under vacuum to RT for 12 hr. to remove water that may have been absorbed during the handling and drilling steps.

Water absorption was monitored gravimetrically versus time by intermittent weighing. Intermittent removal of the specimens from the controlled environments for the brief periods necessary for weighing introduced negligible errors due to the low diffusion coefficients of water in epoxy and the thicknesses of the specimens.

The densities of the different materials were determined in a density gradient column, maintained at 24.5±0.1 °C. The column was calibrated with glass floats of known density. Density specimens were subjected to the same pre-treatment as the water absorption specimens, except they were not drilled.

After removal from the vacuum oven, they were stored in a test tube with desiccant at 24.5°C for eight hours before the density measurements were made.

4. Glass Transition Measurements

T_g determinations were made at about 1 Hz with the torsion braid analyzer (TBA) technique, which uses supported specimens (24). The instrument was also used as a conventional freely-decaying torsion pendulum (TP) using thin films of cured material instead of supported specimens (Fig. 1) (25). When used as a TP, transition temperatures and quantitative values of the modulus are obtained. Fig. 1 is a plot of the shear modulus vs. temperature for a partially-cured and then post-cured film. T_g increases on post-cure, but the RT modulus of the post-cured material is lower than the RT modulus of the partially-cured specimen.

RESULTS

1. Difunctional System

a. Fully-cured Specimens

The raw data for specimens of one of the three fully-cured systems (166°C, 72 hr) are plotted as percentage weight gain of water vs. $(\text{time})^{1/2}/\text{thickness}$ for different RHs (Fig. 4). For clarity, only one of the two specimens per RH is shown. Data for the two duplicate specimens generally showed excellent agreement. The solid lines are discussed later. Throughout this report, only representative figures are shown. The remaining figures, for all of the different cure conditions and materials, are included elsewhere (20). The data are plotted against $(\text{time})^{1/2}/\text{thickness}$ to account for the

different thicknesses of the specimens. Measurements were recorded for approximately 4000 hr. The equilibrium values of the moisture gains vs. RH for the three fully cured systems are included in Table II and are presented in Fig. 5. The T_gs for the three systems (Table II) are not identical, which is an indication that the extent of cure in fact increases slightly as the temperature of cure increases. The initial RT densities of the specimens after cure decrease with increasing temperature of cure (Table II) presumably as a consequence of: 1) the extra cure at higher temperatures; and 2) the lower density of the reactants at higher temperatures. The equilibrium water absorption increases with increasing cure temperature, which corresponds to the trend in RT densities.

b. Partially-cured Specimens

For the specimens cured at 161°C, the expected rise in T_g and decrease in RT density (Table III, Fig. 6) with increasing time of cure were observed. T_gs as determined from supported specimens (TBA) and from thin films (TP) cured with the water absorption specimens were virtually identical (Table III, Fig. 6). The T_g of the specimen cured at 161°C for 341 hr. was 161°C, which is above the $T_{g\infty}$ of 156°C (see earlier). The RT density of this specimen actually shows an increase over the 161°C/72 hr. cure (Table III, Fig. 6). Thus, physical aging, which can occur by annealing at or below T_g (26), or chemical degradation (27) may have occurred during the prolonged cure at 161°C.

As before, the raw data for specimens with one of the six extents of cure (161°C, 5 hr) are plotted as percentage moisture gain vs.

(time)$^{1/2}$/thickness (Fig. 7). Once again, only data for one of the two specimens per RH are plotted. The solid lines are discussed later. Measurements were recorded for approximately 7000 hr. The equilibrium weight gains vs. RH are included in Table III and are presented in Fig. 8.

Two other ways of summarizing the equilibrium results are also informative. The equilibrium moisture gains (M_∞) are plotted against cure time (Fig. 9) and against the dry polymer T_g (Fig. 10) for the different RHs. M_∞ increases with cure time and with T_g, but in both cases M_∞ levels off at very high extents of cure. If the data for the longest cure times were not included, then M_∞ would appear to increase dramatically as T_g approached $T_{g\infty}$ (Fig. 10). This behavior was seen earlier (8), but 24 hr. was the longest cure time used in the previous study. The necessity of studying a wide range of extents of cure is thus evident.

After conditioning in humid environments at 24.5°C for almost one year, the specimens from two cure times were held under vacuum at 100°C in an attempt to find out if the water sorbed could be removed. The weight losses stabilized after 270 hr. at 100°C; the weights after desorption were nearly identical to, but generally greater than, the original weights, with an average difference of 2×10^{-4} gm of water, independent of RH. The analytical balance could be read to 1×10^{-4} gm.

2. Trifunctional System

For the XD7342/TMAB system, T_g and RT density vs. cure time (Fig. 11 and Table IVa) are as expected. The T_g for the 195°C/240 hr. cure reaches the $T_{g\infty}$ of 268°C. (The specimens for the density measurements and water absorption measurements were made from different master batches.)

The raw data for water absorption for specimens with one of the six different extents of cure at 195°C (24 hr), for the 24.5 (Fig. 12a) and 35.0°C (Fig. 12b) exposures, are plotted in the usual way. Measurements were recorded for approximately one year. The equilibrium data for the two temperatures are also tabulated and plotted (Tables IVa and IVb, Figs. 13a and 13b). Two results are immediately obvious: the XD7342 systems absorb significantly more water than the DER 337 resins (cf. Tables II, III, IVa and IVb; Figs. 5, 8, 13a and 13b), and the XD7342 specimens at 24.5°C absorb more water than those at 35.0°C (cf. Tables IVa and IVb; Figs. 13a and 13b). The decrease in equilibrium water absorption (at constant pressure) with an increase in the temperature of exposure has been reported previously (28,29) and is consistent with Le Chatelier's principle because of the exothermic nature of water sorption in epoxies.

The difference in equivalent weights between the di- and trifunctional epoxies may help explain the substantially higher values of M_{∞} for the latter resin. On a 100 gm basis, the difunctional system contains 76 gm DER 337 and 24 gm TMAB, whereas the trifunctional system contains 67 gm XD7342 and 33 gm TMAB. In a fully cured network, DER337 contains about 2.6 moles OH groups per mole epoxy, or about 0.40 moles OH per 100 gm polymer. The corresponding value for XD7342 is 0.42 moles OH per 100 gm polymer. Thus, the contributions from the epoxies are approximately equivalent. However, the trifunctional material has 37.5% more TMAB by weight, which can significantly increase the polarity of the material, and hence the water absorption (8).

The equilibrium data for the two temperatures (24.5 and 35.0°C) are also plotted against cure time (Figs. 14a and 14b) and against the dry polymer T_g

(Figs. 15a and 15b) for the different RHs. The same general trends as observed with the difunctional system are seen, except the equilibrium weight gains do not appear to level off. This is an indication that after 240 hr. at 195°C changes due to cure are still occurring in the trifunctional resin.

DISCUSSION

1. Equilibrium Sorption

The sorption isotherms, which are plots of M_∞ vs. RH or penetrant pressure, yield information on the interaction between the polymer and the penetrant. The adsorption of water by polymers has been the subject of several reviews (28,30,31). The isotherms found in the present work (Figs. 5, 8, 13a and 13b) are of the BET type II classification (32). Type II isotherms have been encountered with hydrophilic polymers such as wool and silk; type III isotherms (the isotherm is sloped continuously upward with no inflection point), and even linear isotherms, have been observed with less hydrophilic materials such as poly(methyl methacrylate) and polyethylene (31). Type II (33-35) and type III (36) isotherms have been obtained with water in epoxy resins. Differences in chemical composition, cure history, and exposure conditions account for the different isotherms and the different amounts of moisture absorbed in studies of nominally similar epoxy resins.

One of the most common approaches to quantifying sorption isotherms has been the BET theory, as described by Brunauer (32). The theory allows for localized multilayer adsorption of gases and vapors on solids, and it

assumes that the same forces that are active in condensation also produce physical adsorption. All molecules in the second and higher layers are assumed equivalent to the liquid state, and different from the first layer. The attraction between adsorbent and adsorbate is of short range, and does not extend beyond the first molecular layer. The BET theory has been severely criticized, but it is still useful in surface area determinations.

A modification of the original BET theory included the assumption that, if adsorption did not take place on a free surface, but in a confined area (as in the interior of a solid), then only a finite number of layers can be adsorbed (32):

$$V = \frac{V_m cx}{1-x} \; \frac{1-(n+1)x^n + nx^{n+1}}{1+(c-1)x - cx^{n+1}} \qquad (1)$$

where V = amount of penetrant adsorbed, gm/100 gm polymer

V_m = amount adsorbed in a monolayer, gm/100 gm polymer

c = BET constant

x = vapor pressure of penetrant/saturation pressure of penetrant at a given temperature

n = maximum number of adsorbed layers on the wall of the confined region

If $n = \infty$, Eq. 1 reduces to the original BET theory, and if $n = 1$, Eq. 1 reduces to the Langmuir isotherm. Equation 1 was applied to the trifunctional resin for which data at different temperatures were available; it was able to fit the data at one temperature with the value of n between 5 and 6, but the

temperature-dependence of the sorption process could not be predicted by the BET theory (Fig. 16). The method of predicting the temperature dependence was taken from the work of Brunauer (32) (see also ref. 9). In Fig. 16, the solid lines represent Eq. 1 at 24.5°C, for different values of n, and the dashed lines represent Eq. 1 at 35°C, with the parameters (C, V_m, and n) derived from the data at 24.5°C. The theory predicts a very slight decrease in adsorption with increase in temperature, but not as much decrease as is seen experimentally.

In the BET theory, the penetrant is localized at specific sites. A more realistic and widely used approach for characterizing sorption isotherms of polymers is the dual mode theory, which is based on moisture being absorbed in glassy polymers in two forms: mobile water and bound water (37). The mobile phase is considered to be described by Henry's law dissolution throughout the polymer matrix whereas the bound or immobilized phase is described by a Langmuir-type adsorption isotherm at specific sites. However, the nature of the immobilizing sites is not known, and could consist of microvoids or other, unknown immobilizing mechanisms (37). This theory is quantitatively described by (37):

$$C = C_D + C_H = k_D p + \frac{C_H' b p}{1+bp} \qquad (2)$$

where C = total solubility

C_D = contribution to C from Henry's law mode

C_H = contribution to C from Langmuir-type mode

k_D = Henry's law dissolution constant

b = hole affinity constant

C_H' = hole saturation constant

p = pressure

At low RHs, the experimental sorption isotherms are concave to the pressure axis, which is consistent with the dual mode sorption theory (38). The dual sorption model was therefore applied to the low pressure data, and a nonlinear least squares analysis was used to determine the best values of k_D, C_H' and b for a given system (Fig. 17) (38). These values, for the difunctional partially-cured materials, are shown in Table V, and compare favorably with values found for another epoxy-amine system (34).

The data from the trifunctional resins at the two temperatures can be used to analyze the temperature dependence of the dual sorption theory. The parameters k_D, C_H' and b should all decrease with increasing temperature (38,39) according to the relationship

$$X = X_o \exp(-\Delta H_x/RT) \qquad (3)$$

where X represents k_D, C_H' or b, ΔH_x is the appropriate enthalpy difference, R is the gas constant and T is the absolute temperature. The parameters k_D and C_H' decrease with temperature for all the cure times at 195°C, but b both increases and decreases with temperature, depending upon cure time. Some instances of an increase in b with temperature have been reported (39).

In order to test the predictive capability of the dual mode theory for different temperatures, sorption experiments were carried out at 45.0°C for the system XD7342/TMAB cured at 195°C for 24 hr. The values of the dual mode

parameters for 45.0°C can be predicted from Eq. 3 with the 24.5 and 35.0°C parameters. The comparison between predicted and experimental values at 45.0°C, along with the experimental values at 24.5 and 35.0°C, are shown in Table VI. (The values of ΔH_x for k_D, -11.9 kcal/mole, and C_H', -9.6 kcal/mole, appear to be reasonable [38]). The agreement seems reasonable for k_D and C_H', considering that only two temperatures were used to make the extrapolation. The prediction of b is not as good. A plot of Eq. 2, for the XD7342/TMAB system, cured at 195°C for 24 hr., for the 45.0°C exposure, is shown in Fig. 18. The solid line is for the experimental parameters; the dashed line is for the predicted parameters.

The dual sorption theory, as formulated in Eq. 2, cannot describe an entire isotherm of the nature encountered in the present work (BET type II, Figs. 5, 8, 13a and 13b). This can be shown simply by differentiating C with respect to p twice in Eq. 2, yielding:

$$\frac{\partial^2 C}{\partial p^2} = - \frac{2C_H' b^2}{(1+bp)^3} \qquad (4)$$

Since C_H' and b are always positive, Eqs. 2 and 4 imply no inflection point in a plot of C vs. p. Thus, another mechanism is needed to explain the experimental sorption isotherms, which do show inflection points.

A model that is commonly invoked to explain positive deviations from the simple dual mode theory (Fig. 17) is clustering, which involves the non-random aggregation of penetrant molecules (40-42). Clustering is described quantitatively by:

$$\frac{G_{11}}{V_1} = -\phi_2\left[\frac{\partial(a_1/\phi_1)}{\partial a_1}\right]_{T,p} - 1 \qquad (5)$$

where G_{11}/V_1 = clustering function

ϕ_2 = volume fraction of polymer

ϕ_1 = volume fraction of penetrant

a_1 = penetrant activity

Values of $G_{11}/V_1 > -1$ indicate a tendency for the penetrant to cluster.

The clustering function is determined from an analysis of the equilibrium sorption isotherm, without regard to an absorption model. In the analysis, the penetrant activity is usually equated to p/p_o, where p is the penetrant pressure and p_o the saturation pressure of the penetrant at the same temperature; additivity of volumes is also assumed in evaluating ϕ_1 (41,42). The values of a_1/ϕ_1 vs. a_1, for the difunctional fully-cured systems, are shown in Fig. 19 (symbols). In order to perform the differentiation as called for in Eq. 5, it is convenient to fit the experimental data for a_1/ϕ_1 vs. a_1 to a second-order polynomial (solid lines, Fig. 19), and then differentiate the polynomials analytically. The results of this analysis (Fig. 20) show clearly that $G_{11}/V_1 > -1$ for the three highest RHs studied, which are the RHs for which the dual mode theory fails and where clustering is considered to become important. At low RH, G_{11}/V_1 is a large negative value, which indicates that the water is localized to some degree (40); this fact is consistent with the curvature of the isotherms at low RH (Fig. 17) (34).

NMR evidence has also been presented (33) which indicated that at low concentrations of sorbed moisture (< 1% for the epoxy resin studied), the

water was strongly bound to polar sites in the epoxy matrix. At higher water concentrations, the NMR evidence indicated mobile water was present. (Mobile in this context refers to rotational mobility, not necessarily translational mobility.)

The effect of water vapor on epoxies (43) and polyimides (44) has been investigated by dynamic mechanical techniques; at low water concentrations, a strong polymer-water interaction was detected by the development of a loss peak at cryogenic temperatures, the intensity of which was proportional to the water concentration. At higher levels of water the loss peak height was independent of water concentration, indicating a different mode of sorption.

The values of the clustering function for the trifunctional systems are less than those of the difunctional systems (20), which indicates that clustering is less pronounced in the trifunctional systems; this difference is consistent with the polarity of the trifunctional resins being greater than the difunctional ones.

Thus, a qualitative description of the equilibrium water absorption in epoxy resins emerges by considering dual mode sorption at low RH together with clustering at high RH. At low water activities, simple dual mode sorption can describe the isotherms, which is reinforced by the negative values of the clustering function. At high water activities, the dual mode theory can no longer describe the sorption isotherms, but the clustering function indicates that penetrant clustering is occurring.

Two other approaches to characterizing the sorption isotherms of water in epoxies have been investigated, for the purpose of providing methods for

correlating adsorption data at different temperatures. Both of these approaches are thermodynamic in nature.

In both theories, the adsorbate is considered to behave as a liquid, although the properties of the adsorbate may differ from those of the bulk liquid at the same temperature because of the influence of the adsorbent. In the first theory, the difference in free energy between the adsorbate and its saturated liquid at the same temperature is referred to as the adsorption potential ϵ (45):

$$\epsilon = RT\ell n(p_o/p) \qquad (6)$$

For a given adsorbent-adsorbate system, a unique temperature-independent relationship exists between ϵ and the volume of penetrant adsorbed. The resulting plot of ϵ vs. the volume adsorbed is known as the characteristic curve. At temperatures below the normal boiling point of the adsorbate, the liquid density is usually used in calculating the volume adsorbed (45). Although there appears to be little theoretical justification for the application of this theory to polar systems, the theory has been applied with some success to them (45).

The characteristic curve approach was applied to the trifunctional resins, and good agreement with the theory was observed for the three temperatures studied for one degree of cure (Fig. 21). The theory was also applied to some reported data on water absorption in epoxies (46), which examined temperatures from 0.2 to 90°C. At high temperatures, moisture may damage an epoxy resin, thus inducing different mechanisms of water absorption.

If only the data from 25 to 70°C are examined, the data fall on one curve (Fig. 22). An advantage of the characteristic curve approach is that the level of adsorption at different temperatures can be predicted from one experimental isotherm, without regard to a specific adsorption model.

The second thermodynamic approach accounts for the polarizability of the water. The adsorption potential is now described by (47):

$$\epsilon = RT\ln(p_o/p) = c_1 e^{-c_2 V_\ell \phi} \qquad (7)$$

where ϕ = volume of penetrant adsorbed

V_ℓ = molar volume of penetrant

c_1, c_2 = constants

Thus, a plot of $\ln[RT\ln(p_o/p)]$ vs. $V_\ell\phi$ should yield a straight line independent of temperature. Eq. 7 was applied to the results on the trifunctional resin, and good agreement was found up to 90% RH (Fig. 23). This polarization model has also been successful with other water-adsorbent systems (48).

2. Transient Sorption

The simplest model for moisture diffusion in epoxies is described by Fick's equation for one-dimensional diffusion with constant diffusion coefficient:

$$\frac{\partial c}{\partial t} = D \frac{\partial^2 c}{\partial x^2} \tag{8}$$

where D is the diffusion coefficient normal to the surface and c is the concentration of moisture. One-dimensional diffusion is justified in this case because the length and width of the specimens are considerably greater than the thickness. Eq. 8 can be solved analytically and integrated over the thickness to provide the weight gain as a function of time (49):

$$M(t) = M_\infty \left[1 - \frac{8}{\pi^2} \sum_{j=0}^{\infty} \frac{\exp\left[-(2j+1)^2 \pi^2 \left(\frac{Dt}{(2a)^2}\right)\right]}{(2j+1)^2}\right] \tag{9}$$

where $M(t)$ = moisture content at time t

$2a$ = specimen thickness.

To account for non-uniform specimen thicknesses, an average specimen thickness was calculated:

$$2a = \frac{W_i}{\ell w \rho} \tag{10}$$

where W_i = initial specimen weight

ℓ = specimen length

w = specimen width

ρ = specimen density

Nominal diffusion coefficients were calculated from the initial slopes of the lines in Figs. 4, 7, 12a and 12b using the following equation:

$$D = \pi \left(\frac{m[2a]}{4M_\infty}\right)^2 \qquad (11)$$

where m = slope of linear portion of M(t) vs. $(time)^{1/2}$/thickness (49). The nominal diffusion coefficients for the difunctional systems were in the range 1-2 x 10^{-9} cm^2/sec; for the trifunctional systems at 24.5°C, 0.8-1.5 x 10^{-9} cm^2/sec; and for the trifunctional systems at 35.0°C, 1.3-2.5 x 10^{-9} cm^2/sec. As the extent of cure increases (and thus crosslinking increases), the diffusion coefficient appears to decrease. This is the reported trend for diffusion in crosslinked polymers (30,50,51). The diffusion coefficient also appears to decrease with an increase in RH.

The diffusion coefficients of the difunctional resins are generally higher than the diffusion coefficients of the trifunctional materials, which can be understood in terms of the higher crosslinking and polarity of the trifunctional systems. The diffusion coefficients are also higher at 35.0°C than at 24.5°C for the trifunctional systems.

It should be noted that the determination of the sorption kinetics from data derived from intermittent specimen weighing is not an ideal approach (30,52,53). Thus, no quantitative conclusions regarding the relationships between the diffusion coefficients and cure time and water activity are drawn, although general trends can be described. The errors in the equilibrium values are minor.

An alternative explanation for the RT free volume and equilibrium water absorption increasing with increasing extent of cure could be that at higher extents of cure greater stresses are introduced into the material upon cooling to RT, and that microcracks develop. However, the decrease in the diffusion coefficient with extent of cure is an argument against this hypothesis, because cracks would be expected to dramatically increase the diffusion coefficient.

Eq. 9 can be plotted and compared to data for representative specimens (solid lines, Figs. 4, 7, 12a and 12b). There is a good match between the model (Eq. 9) and the experimental data at low RH (11%, 29% and 43%). However, at the higher RHs the sorption process is slower than the model predictions, which is an indication that simple Fickian diffusion (Eq. 8) is no longer applicable. (For the thicknesses and diffusion coefficients under consideration, Eq. 9 converges rapidly for all but very small times; there is no need for an analytical approximation to Eq. 9.)

A more appropriate diffusion model should account for water existing in epoxy resins in both bound and mobile forms, as discussed in connection with the dual mode theory in the previous section. Thus, Eq. 8 should be modified to account for the bound population:

$$\frac{\partial C_D}{\partial t} + \frac{\partial C_H}{\partial t} = D \frac{\partial^2 C_D}{\partial x^2} \qquad (12)$$

where C_D and C_H have the same meaning as in the previous section. Eq. 12 can be solved for the particular case of C_D and C_H being in local equilibrium throughout the polymer.

A general model, which includes Eq. 12 as a special case, relaxes the assumption that C_D and C_H are always in local equilibrium. Some recent studies have proposed the following model (54-58) for the diffusion of water:

$$\frac{\partial C_D}{\partial t} + \frac{\partial C_H}{\partial t} = D \frac{\partial^2 C_D}{\partial x^2} \tag{13a}$$

$$\frac{\partial C_H}{\partial t} = \lambda C_D - \mu C_H \tag{13b}$$

where λ = rate constant for the forward process of $C_D \rightleftharpoons C_H$, and μ = rate constant for the reverse process. The clustering process is one cause of slow immobilization of penetrant, which requires the use of Eq. 13b along with Eq. 13a. In Eqs. 13a and 13b, the immobilization process is not necessarily rapid compared with diffusion, whereas the use of Eq. 12 alone considers that immobilization is very rapid compared to diffusion.

Eqs. 13a and 13b can be solved analytically, with the following initial and boundary conditions:

$$C_D(x,0) = C_H(x,0) = 0 \qquad -a \leq x \leq a,\ t = 0 \tag{14a}$$

$$C_D(a,t) = C_\infty \qquad x = a,\ t > 0 \tag{14b}$$

$$\frac{\partial C_D}{\partial x}(0,t) = 0 \qquad x = 0,\ t > 0 \tag{14c}$$

where C_∞ is the surface concentration of the penetrant and 2a is the film thickness. The complete solution is (49):

$$\frac{M(t)}{M_\infty} = 1 - \frac{2}{R+1} \left\{ \sum_{n=0}^{\infty} \frac{(R+1+C_3^+)^2 \exp[C_1 C_2 C_3^+ (R+1)]}{\pi^2 (n+\frac{1}{2})^2 ((1+C_3^+)^2 + R)} \right.$$

$$+ \sum_{n=0}^{\infty} \frac{(R+1+C_3^-)^2 \exp[C_1 C_2 C_3^- (R+1)]}{\pi^2 (n+\frac{1}{2})^2 ((1+C_3^-)^2 + R)} \Bigg\} \qquad (15)$$

where

$$R = \frac{\lambda}{\mu}$$

$$C_1 = \frac{\mu a^2}{D}$$

$$C_2 = \frac{Dt}{(R+1)a^2}$$

$$C_3^{\pm} = \frac{1}{2} \left\{ -\left(R+1 + \frac{(n+\frac{1}{2})^2 \pi^2}{C_1}\right) \pm \left[\left(R+1 + \frac{(n+\frac{1}{2})^2 \pi^2}{C_1}\right)^2 - \frac{4(n+\frac{1}{2})^2 \pi^2}{C_1} \right]^{1/2} \right\}$$

In order to apply Eq. 15, three parameters -- R, λ or μ, and D -- must be known. The sorption isotherms can be used to eliminate one of these parameters, because at equilibrium,

$$\frac{\partial C_H}{\partial t} = 0 = \lambda C_D - \mu C_H \qquad (16)$$

$$R = \frac{\lambda}{\mu} = C_H / C_D$$

Thus, from Eq. 2, $C_D = k_D p$, and $C_H = C - C_D$. It was assumed that the concentration of mobile species, C_D, was represented by $k_D p$, even in the high RH regime where Eq. 2 was no longer valid. In other words, at high RH, the

Langmuir term is modified to account for the clustering, but the Henry's law term remains the same.

With this approach, R was calculated for all the RHs for each cure condition, and a nonlinear least squares analysis was used to calculate D and μ from Eq. 15. The results of this analysis are shown in Figs. 24a and 24b for the difunctional systems, and in Figs. 24c and 24d for the trifunctional systems. The curves generally fit the data at all RHs and cure conditions, for both systems.

The diffusion coefficients calculated from Eq. 15 for the difunctional systems are in the range 2-4 x 10^{-9} cm^2/sec; for the trifunctional systems at 24.5°C, 1.5-2 x 10^{-9} cm^2/sec; and for the trifunctional systems at 35.0°C, 2-3.3 x 10^{-9} cm^2/sec. The diffusion coefficients follow the same patterns as discussed previously, but are significantly larger than the ones calculated from Eq. 11. Thus, failure to account for the immobilized water can lead to erroneously low estimates of the diffusion coefficient (37). The effective diffusion coefficient, as calculated from Eq. 11, is smaller than the real diffusion coefficient, as used in Eq. 13a, because of the immobilization process.

A more complete analysis of the transient sorption process would examine the effect of partial immobilization, and would attempt to incorporate the concentration dependence of the diffusion coefficient into the model. The experimental methods used in this work are not amenable to the more complex analyses. Permeation experiments are generally required to detect evidence of partial immobilization, but sorption experiments can examine the validity of

the assumption of local equilibrium between the mobile and bound populations (59, 60).

3. Extent of Cure vs. Water Absorption

The effect of extent of cure on RT properties of high T_g epoxy resins results in an anomaly observed previously (6-9) and in this work: as extent of cure increases, T_g increases, RT modulus decreases, RT density decreases, and RT water absorption increases. Three other reports in the literature concerning the effect of extent of cure (or crosslinking density) on water absorption in epoxies were examined. The first report concerned tetraglycidyl 4,4'-diaminodiphenyl methane (TGDDM) cured with diaminodiphenyl sulfone (DDS); specimens were cured at four temperatures (149, 175, 203, 231°C) for four different times (1, 3.5, 9, 19.5 hr.) at each temperature (61). The second study dealt with nominally the same resin system, TGDDM/DDS, cured at 150, 177, and 190°C (33). The third paper studied a diglycidyl ether of bisphenol A (Epon 828) cured with a stoichiometric amount of m-phenylenediamine (m-PD)/aniline mixtures (5). In this last report, the crosslinking density varied because m-PD is tetrafunctional whereas aniline is only difunctional.

The conclusions for the four studies are summarized in Table VII. Three of the studies (present study, 61, 5) show that as T_g increases, $M_{x,}$ increases. The different ways of varying the extent of cure must be considered, however. The two studies (present study, 61) that examined isothermal cures for different times both show an increase in $M_{x,}$ with cure time. When extent of cure was varied by curing at different temperatures, conflicting results were

observed (present study, 61, 33). In the present report, there is a trend of increasing M_x with increasing cure temperature (Fig. 5), which was also seen in ref. 61. The RT densities also decrease with cure temperature (present study). This could be accounted for by the fact that the material cured at the highest temperature has the lowest initial density during cure, due to increased thermal fluctuations, and that this is carried over into the RT properties of the fully-cured system (62). The higher temperatures of cure can also lead to more fully cured materials, which can lead to increases in the water absorption, as discussed earlier. It is therefore expected that materials cured at higher temperatures would absorb more water, based on a lower RT density and greater free volume.

In ref. 61, a chemical argument was advanced to account for the increase in M_x with both cure time and cure temperature; as cure increases, the number of hydroxyl sites formed increases, providing more hydroxyl sites for moisture sorption. It is not clear, however, that polarity increases with cure because amine and epoxy groups disappear as hydroxyl groups form.

In ref. 33, a morphological argument was proposed to account for the decrease in M_x with increasing cure temperature; as cure temperature increased, crosslinking density increased, and steric hindrances were considered to limit the accessibility of sorption sites. The decrease in the RT diffusion coefficient (D) with an increase in the extent of cure is consistent with the observations of the present study.

In ref. 5, polarity and other morphological arguments were advanced to explain the increase in M_x and D with the increase in the amount of m-PD

(which leads to increases in T_g and crosslinking density). First, m-PD is more polar than aniline, and increasing the amount of m-PD at the expense of aniline would be expected to increase M_x (the importance of resin polarity on water absorption has been considered [8]). Second, the development of a two-phase morphology (highly crosslinked phase surrounding less crosslinked phase) with increasing concentration of aniline was invoked, and it was proposed that the highly crosslinked phase would slow down or prevent moisture penetration into the less crosslinked sections. The greater density of m-PD compared with aniline contributes to the increase in RT density as T_g increases.

A self-consistent explanation for the present results is that more free volume at RT is trapped in the more highly cured specimens than in the undercured specimens. The excess free volume is manifest in the lower RT densities and modulus (7). Thus, for the same resin subjected to different extents of cure at the same temperature, an explanation of increasing M_x with increasing extent of cure based on increasing free volume at RT leads to a consistent explanation for a number of different phenomena.

The increase in RT free volume with increasing extent of cure appears to be the most important factor in determining M_x, for any given system. However, the diffusion coefficient appears to be controlled not by the increase in free volume, but rather by the increase in crosslinking density, and thus the rate of water absorption decreases with increasing extent of cure.

4. Free Volume Explanation

An earlier study on epoxy/anhydride systems resulted in RT density decreasing with increasing isothermal cure time (11). A schematic diagram of the specific volume vs. temperature is shown in Fig. 25, for a partially-cured specimen (labeled 1) and a more fully-cured specimen (labeled 2), both specimens having been cured isothermally at T_a. Isothermally above T_{g2}, in the rubbery state, the decrease in specific volume (v) with increasing cure is noted.

The total specific volume is made up of two contributions (63):

$$v = v_f + v_o \qquad (17)$$

where v_f = free volume per gram and v_o = occupied volume per gram, which includes the volume of the molecules as represented by van der Waals radii and also the volume associated with thermal vibrations. v_o increases with temperature, and its expansion coefficient is usually equated to α_g, the thermal expansion coefficient of the glassy state (63). In the present simplified analysis, v is assumed to be linear with temperature, so α = constant = dv/dT.

The central question is how $\Delta v_g/\Delta T_g$ (dashed line, Fig. 25) is related to the polymer structure, and how it is influenced by cure, where v_g is the specific volume at T_g. Proceeding analogously to Shimazaki (11), at an arbitrary temperature T_a above T_{g2}:

$$v_{1a} = v_{o1} + v_{f1} = v_{g1} + \alpha_\ell(T_a - T_{g1}) \tag{18}$$

where $\alpha_\ell = (v_{1a} - v_{g1})/(T_a - T_{g1})$ = liquid thermal expansion coefficient.

Also

$$v_{2a} = v_{o2} + v_{f2} = v_{o1} - \Delta v_o + v_{f1} - \Delta v_f$$

$$= v_{g2} + \alpha_\ell(T_a - T_{g2}) \tag{19}$$

As defined here, Δv_o and Δv_f are both positive. From physical considerations, it is reasonable to assume v_o decreases on further cure, since crosslinking ties up free ends and constrains thermal vibrations. Now from Eqs. 18 and 19:

$$v_{g1} = v_{o1} + v_{f1} - \alpha_\ell(T_a - T_{g1}) \tag{20a}$$

$$v_{g2} = (v_{o1} - \Delta v_o) + (v_{f1} - \Delta v_f) - \alpha_\ell(T_a - T_{g2}) \tag{20b}$$

Subtracting v_{g1} from v_{g2} yields:

$$v_{g2} - v_{g1} = -(\Delta v_o + \Delta v_f) + \alpha_\ell(T_{g2} - T_{g1}) \tag{21}$$

Therefore:

$$B \equiv \frac{v_{g2} - v_{g1}}{T_{g2} - T_{g1}} = - \frac{\Delta v_o + \Delta v_f}{T_{g2} - T_{g1}} + \alpha_\ell \qquad (22)$$

The slope of B depends on the relative magnitudes of $-(\Delta v_o + \Delta v_f)$ and α_ℓ, since Δv_o and Δv_f will always be positive for additional reaction or crosslinking (occupied volume and free volume will always decrease in the rubbery state) (11). In a qualitative sense, the sign of B can be predicted to determine if the inverse relationship between T_g and RT density will be observed. For the epoxy system under consideration, the free volume cannot decrease too much because of the bulky chains present (11), and thus Δv_o and Δv_f are small positive values, so $\alpha_\ell - (\Delta v_o + \Delta v_f)/(T_{g2} - T_{g1}) > 0$. If a more flexible system were under study, then Δv_f could decrease enough so that B had a negative slope. Shimazaki referred to a flexible system when he gave an example of a system with $B < 0$ (glyceryl isophthalate resin modified with linseed oil) (11). Qualitatively, therefore, systems which are composed of rigid molecules, or possess other hindrances, would be expected to exhibit the inverse relationship between T_g and RT density, because in the equilibrium state above T_g the decrease in free volume upon further cure is restricted.

CONCLUSIONS

In this study, the effect of different time-temperature paths of cure on the RT density and water absorption behavior of di- and trifunctional high T_g epoxy resins has been investigated. The difunctional system, DER 337/TMAB, had a lower T_g than the standard epoxy cured with TMAB, allowing full cure while minimizing complications due to thermal degradation.

The difunctional resin was cured at three temperatures; the higher the cure temperature, the lower the RT density and the higher the value of the equilibrium water gain (M_∞). The initial temperature of cure appears to be important in determining RT properties.

The resins were also cured isothermally for different times. The following trends were observed: as extent of cure increased, T_g increased, RT density decreased, the RT diffusion coefficient (D) appeared to decrease, and M_∞ increased. The free volume is considered to control M_∞, whereas the crosslink density appears to control the rate of water absorption. The decrease in D with increase in extent of cure lends support to the idea that the increase in RT free volume determines M_∞, rather than the increased presence of microcracks with cure. The increase in RT free volume can be explained qualitatively by a restricted decrease in free volume above T_g due to the rigidity of the molecules involved. Systems consisting of flexible molecules would be expected to show a decrease in RT free volume with increasing cure or extent of reaction.

The sorption isotherms were examined in detail, and can be described by the dual mode theory at low RH and clustering at high RH. The transient and equilibrium data support the hypothesis of penetrant clustering at high RH. An empirical thermodynamic approach was also investigated, which correlated sorption data at different temperatures successfully.

ACKNOWLEDGMENT

This research was supported by the Army Research Office and the Office of Naval Research.

REFERENCES

1. R. J. Morgan, J. E. O'Neal, and D. L. Fanter, J. Mat. Sci., 15, 751 (1980).

2. C. E. Browning, Polym. Eng. Sci., 18(1), 16 (1978).

3. I. D. Maxwell and R. A. Pethrick, J. Appl. Polym. Sci., 28, 2363 (1983).

4. M. Continaud, P. Bonniau, and A. R. Bunsell, J. Mat. Sci., 17, 867 (1982).

5. Y. Diamant, G. Marom, and L. J. Broutman, J. Appl. Polym. Sci., 26, 3015 (1981).

6. J. P. Aherne, J. B. Enns, M. J. Doyle, and J. K. Gillham, ACS, Div. Org. Coat. Plast. Chem. Prep., 46, 574 (1982).

7. J. B. Enns and J. K. Gillham, J. Appl. Polym. Sci., 28, 2831 (1983).

8. M. T. Aronhime, J. K. Gillham, and R. D. Small, ACS, Div. Polym. Mat.: Sci. Eng. Prep., 49, 576 (1983).

9. M. T. Aronhime, X. Peng, J. K. Gillham, and R. D. Small, ACS, Div. Polym. Mat.: Sci. Eng. Prep., 51, 436 (1984).

10. S. Mostovoy and E. J. Ripling, J. Appl. Polym. Sci., 10, 1351 (1966).

11. A. Shimazaki, J. Polym. Sci., Part C, 23, 555 (1968).

12. K. Ueberreiter and G. Kanig, J. Colloid Sci., 7, 569 (1953).

13. E. Kiran, J. K. Gillham, and E. Gipstein, J. Macromol. Sci.-Phys., B9(2), 341 (1974).

14. G. A. Pogany, Eur. Polym. J., 6, 343 (1970).

15. N. Hata and J. Kumanotani, J. Appl. Polym. Sci., 15, 2371 (1971).

16. N. Hata, R. Yamauchi and J. K. Kumanotani, J. Appl. Polym. Sci., 17, 2173 (1973).

17. J. Daly, A. Britten, A. Garton and P. D. McLean, J. Appl. Polym. Sci., 29, 1403 (1984).

18. R. F. Boyer, Polymer, 17, 996 (1976).

19. J. S. Osinski and L. T. Manzione, in Epoxy Resin Chemistry II, R. S. Bauer, Ed., ACS Symp. Ser. 221, 263 (1983).

20. M. T. Aronhime, Ph.D. Thesis, Princeton University, June 1985.

21. J. B. Enns and J. K. Gillham, in Polymer Characterization, C. D. Craver, Ed., ACS Adv. Chem. Ser. 203, 27 (1983).

22. Epoxy Resin Comparative Data Manual, The Dow Chemical Co., Plastics Department (1979).

23. R. R. Jay, Anal. Chem., 36(3), 667 (1964).

24. J. K. Gillham, in Developments in Polymer Characterisation-3, J. V. Dawkins, Ed., Applied Science Publishers, Ltd., London, 1982, Ch. 5.

25. J. B. Enns and J. K. Gillham, in Computer Applications in Applied Polymer Science, T. Provder, Ed., ACS Symp. Ser. 197, 329 (1982).

26. L. C. E. Struik, Polym. Eng. Sci., 17 (3), 165 (1977).

27. L. C. Chan, H. N. Naé, and J. K. Gillham, J. Appl. Polym. Sci., 29, 3307 (1984).

28. A. D. McLaren and J. W. Rowen, J. Polym. Sci., 7(2/3), 289 (1951).

29. P. Moy and F. E. Karasz, in Water in Polymers, S. P. Rowland, Ed., ACS Symp. Ser. 127, 505 (1980).

30. R. M. Felder and G. S. Huvard, in Methods of Experimental Physics, Vol. 16, Part C, R. A. Fava, Ed., Academic Press, New York, 1980.

31. J. A. Barrie, in Diffusion in Polymers, J. Crank and G. S. Parke, Eds., Academic Press, New York, 1968, Ch. 8.

32. S. Brunauer, The Adsorption of Gases and Vapors, Vol. 1, Oxford University Press, London, 1944.

33. P. Moy and F. E. Karasz, Polym. Eng. Sci., 20(4), 315 (1980).

34. J. A. Barrie, P. S. Sagoo and P. Johncock, J. Membrane Sci., 18, 197 (1984).

35. A. Apicella, R. Tessieri and C. DeCataldis, J. Membrane Sci., 18, 211 (1984).

36. J. Comyn, D. M. Brewis, R. J. A. Shalash and J. L. Tegg, in Adhesion, Vol. 3, K. W. Allen, Ed., Applied Science Publishers, Ltd., London, 1979, p. 13.

37. W. R. Vieth, J. M. Howell and J. H. Hsieh, J. Membrane Sci., 1, 177 (1976).

38. G. Ranade, V. Stannett and W. J. Koros, J. Appl. Polym. Sci., 25, 2179 (1980).

39. G. R. Mauze and S. A. Stern, J. Membrane Sci., 12, 51 (1982).

40. B. H. Zimm and J. L. Lundberg, J. Phys. Chem., 60, 425 (1956).

41. J. L. Lundberg, J. Macromol. Sci.-Phys., B3(4), 693 (1969).

42. V. Stannett, M. Haider, W. J. Koros and H. B. Hopfenberg, Polym. Eng. Sci., 20(4), 300 (1980).

43. J. K. Gillham, C. A. Glandt and C. A. McPherson, in Chemistry and Properties of Crosslinked Polymers, S. S. Labana, Ed., Academic Press, Inc., N.Y., 1977, p. 491.

44. Y. Ozari, R. H. Chow and J. K. Gillham, J. Appl. Polym. Sci., 23, 1189 (1979).

45. D. M. Ruthven, Principles of Adsorption and Adsorption Processes, John Wiley & Sons, Inc., New York, 1984.

46. B. Ellis and H. U. Rashid, J. Appl. Polym. Sci., 29, 2021 (1984).

47. A. W. Adamson, Physical Chemistry of Surfaces, 3rd Ed., John Wiley & Sons, Inc., New York, 1976.

48. G. N. Ling, in Water Structure at the Water-Polymer Interface, Plenum Press, New York, 1972, p. 4.

49. J. Crank, The Mathematics of Diffusion, Oxford University Press, London, 1956.

50. V. Stannett, in Diffusion in Polymers, J. Crank and G. S. Parke, Eds., Academic Press, New York, 1968, Ch. 2.

51. R. P. Chartoff and T. W. Chiu, Polym. Eng. Sci., 20(4), 244 (1980).

52. R. Blahnik, Prog. Org. Coat., 11, 353 (1983).

53. D. Y. Perera and P. Selier, Prog. Org. Coat., 1, 57 (1973).

54. H. G. Carter and K. G. Kibler, J. Comp. Mat., 12, 118 (1978).

55. W. Vieth, A. S. Douglas and R. Bloch, J. Macromol. Sci.-Phys., B3(4), 737 (1969).

56. M. E. Gurtin and C. Yatomi, J. Comp. Mat., 13, 126 (1978).

57. B. Dewimille and A. R. Bunsell, J. Phys. D: Appl. Phys., 15, 2079 (1982).

58. M. S. Majerus, D. S. Soong and J. M. Prausnitz, J. Appl. Polym. Sci., 29, 2453 (1984).

59. J. H. Petropoulos, J. Polym. Sci.: A-2, 8, 1797 (1970).

60. R. A. Assink, J. Polym. Sci.: Polym. Phys. Ed., 13, 1665 (1975).

61. N. D. Danieley and E. R. Long, Jr., J. Polym. Sci.: Polym. Chem. Ed., 19, 2443 (1981).

62. M. B. Roller, J. Coat. Tech., 54(691), 33 (1982).

63. J. D. Ferry, Viscoelastic Properties of Polymers, 3rd Ed., John Wiley & Sons, Inc., New York, 1980.

64. J. F. Young, J. Appl. Chem., 17, 241 (1967).

LIST OF TABLES

FIGURE CAPTIONS

Fig. 1. Shear modulus (torsion pendulum) vs. temperature of partially-cured DER337/TMAB (161°C/3 hr) specimen: 140→-170→240→-170°C, 1.5°C/min. Note that the RT modulus is decreased by post-cure.

Fig. 2. Chemical formulae of the materials used in this study. For DER337, n = 0.6.

Fig.3a. Isothermal time-temperature-transformation (TTT) cure diagram of DER337/TMAB: temperature of cure vs. times to gelation (■) and vitrification (○); $T_{g\infty}$ (dotted line).

Fig.3b. Isothermal time-temperature-transformation (TTT) cure diagram of XD7342/TMAB: temperature of cure vs. times to gelation (■) and vitrification (○); $T_{g\infty}$ (dotted line).

Fig. 4. Percent moisture gain at 24.5°C vs. time$^{1/2}$/thickness for different relative humidities for DER337/TMAB (166°C/72 hr cure): experimental (symbols); Eq. 9 (solid lines).

Fig. 5. Equilibrium moisture gain at 24.5°C vs. relative humidity for DER337/TMAB (fully-cured systems).

Fig. 6. Room temperature density and T_g vs. cure time for DER337/TMAB (partially-cured systems [161°C]): density (□); T_g as determined in TBA experiment (○); T_g as determined in TP experiment (△).

Fig. 7. Percent moisture gain at 24.5°C vs. time$^{1/2}$/thickness for different relative humidities for DER337/TMAB (161°C/5 hr cure): experimental (symbols); Eq. 9 (solid lines).

Fig. 8. Equilibrium moisture gain at 24.5°C vs. relative humidity for

DER337/TMAB (partially-cured systems [161°C]).

Fig. 9. Equilibrium moisture gain at 24.5°C vs. cure time for DER337/TMAB (partially-cured systems [161°C]).

Fig. 10. Equilibrium moisture gain at 24.5°C vs. dry polymer T_g for DER337/TMAB (partially-cured systems [161°C]).

Fig. 11. Room temperature density and T_g vs. cure time for XD7342/TMAB (partially-cured systems [195°C]): density (■); T_g as determined in TBA experiment (◇).

Fig. 12a Percent moisture gain at 24.5°C vs. time$^{1/2}$/thickness for different relative humidities for XD7342/TMAB (195°C/24 hr cure): experimental (symbols); Eq. 9 (solid lines).

Fig. 12b Percent moisture gain at 35.0°C vs. time$^{1/2}$/thickness for different relative humidities for XD7342/TMAB (195°C/24 hr cure): experimental (symbols); Eq. 9 (solid lines).

Fig. 13a Equilibrium moisture gain at 24.5°C vs. relative humidity for XD7342/TMAB (partially-cured systems [195°C]).

Fig. 13b Equilibrium moisture gain at 35.0°C vs. relative humidity for XD7342/TMAB (partially-cured systems [195°C]).

Fig. 14a Equilibrium moisture gain at 24.5°C vs. cure time for XD7342/TMAB (partially-cured systems [195°C]).

Fig. 14b Equilibrium moisture gain at 35.0°C vs. cure time for XD7342/TMAB (partially-cured systems [195°C]).

Fig. 15a Equilibrium moisture gain at 24.5°C vs. T_g for XD7342/TMAB (partially-cured systems [195°C]).

Fig. 15b Equilibrium moisture gain at 35.0°C vs. T_g for XD7342/TMAB

(partially-cured systems [195°C]).

Fig. 16 BET analysis for different values of n for XD7342/TMAB (195°C/96 hr): three parameter BET model (Eq. 1) for 24.5°C data (solid lines); three parameter BET model (Eq. 1) for 35.0°C data using parameters derived from 24.5°C data (dashed lines).

Fig. 17 Equilibrium moisture gain at 24.5°C vs. pressure for DER337/TMAB (161°C/29 hr cure): experimental (symbols); dual mode theory (Eq. 2) (solid line).

Fig. 18 Equilibrium moisture gain at 45.0°C vs. pressure for XD7342/TMAB (195°C/24 hr cure): experimental (□); dual mode theory (Eq. 2) with experimental parameters (solid line); dual mode theory (Eq. 2) with predicted parameters (dashed line).

Fig. 19 Penetrant activity/volume fraction at 24.5°C vs. penetrant activity for DER337/TMAB (fully-cured systems): experimental (symbols); best second-order polynomial (solid lines).

Fig. 20 Cluster function (G_{11}/V_1) at 24.5°C vs. penetrant activity for DER337/TMAB (fully-cured systems).

Fig. 21 Adsorption potential (ϵ) vs. volume of penetrant adsorbed for XD7342/TMAB (195°C/24 hr cure) for three temperatures.

Fig. 22 Adsorption potential (ϵ) vs. volume of penetrant adsorbed for data of Ellis and Rashid (46) for five temperatures.

Fig. 23 Ln (adsorption potential) vs. penetrant molar volume x volume of penetrant adsorbed for XD7342/TMAB (195°C/24 hr cure) for three temperatures.

Fig. 24a Percent moisture gain at 24.5°C vs. time$^{1/2}$/thickness for different relative humidities for DER337/TMAB (166°C/72 hr cure): experimental (symbols); Eq. 15 (solid lines). Compare with Fig. 4.

Fig. 24b Percent moisture gain at 24.5°C vs. time$^{1/2}$/thickness for different relative humidities for DER337/TMAB (161°C/5 hr cure): experimental (symbols); Eq. 15 (solid lines). Compare with Fig. 7.

Fig. 24c Percent moisture gain at 24.5°C vs. time$^{1/2}$/thickness for different relative humidities for XD7342/TMAB (195°C/24 hr cure): experimental (symbols); Eq. 15 (solid lines). Compare with Fig. 12a.

Fig. 24d Percent moisture gain at 35.0°C vs. time$^{1/2}$/thickness for different relative humidities for XD7342/TMAB (195°C/24 hr cure): experimental (symbols); Eq. 15 (solid lines). Compare with Fig. 12b.

Fig. 25 Schematic. Specific volume vs. temperature for partially-cured and fully-cured materials, showing effect of extent of cure on specific volume in the rubbery state (above T_{g2}) and the glassy state (below T_{g1}). See text for description of variables. v_{f_1} and v_{f_2} are free volumes for the different extents of cure at T_a.

TABLE I

Relative Humidity Values from Saturated Salt Solutions

	Relative Humidity (%)		
Salt	24.5°C[a]	35°C[a]	45°C[a]
$LiCl \cdot H_2O$	11	11	11
$CaCl_2 \cdot 6H_2O$	29	21	17
$K_2CO_3 \cdot 2H_2O$	43.5	43	42
$Mg(NO_3)_2 \cdot 6H_2O$	53	50	47
NH_4Cl	78	75	73
$BaCl_2 \cdot 2H_2O$	90	89.5	89
$NH_4H_2PO_4$	93	91.5	90

a From ref. 64, p. 242.

TABLE II

Summary of Data for DER 337/TMAB: Fully-Cured Systems

	Equilibrium moisture gain(%)		
Relative Humidity(%)	131°C/168 hr.*	145°C/96 hr.*	166°C/72 hr.*
11	0.3130	0.3615	0.3677
29	0.6623	0.7476	0.7850
43	0.9559	1.0411	1.0728
53	1.1570	1.2857	1.3328
78	1.7260	1.9111	1.9511
90	2.0709	2.3450	2.4159
93	2.1795	2.4424	2.5130
RT Density (gm/cc)	1.2121	1.2118	1.2114
T_g (°C, TBA)	153	155	156

*Cure conditions for fully-cured systems.

TABLE III

Summary of Data for DER337/TMAB: Partially-Cured Systems (161°C)

Relative Humidity(%)	Equilibrium Moisture Gain (%) 3 hr.*	5 hr.*	11 hr.*	29 hr.*	72 hr.*	341 hr.*
11	0.2730	0.3183	0.3490	0.3634	0.3595	0.3585
29	0.6533	0.6933	--	0.7809	0.7972	0.8023
43	0.8962	0.9840	1.0409	1.1210	1.1241	1.1132
53	1.0869	1.1874	1.2763	1.3247	1.3510	1.3486
78	1.6579	1.7798	1.9394	1.9908	2.0586	2.0118
90	2.0523	2.2312	2.4065	2.4731	2.4583	2.5166
93	2.1533	2.3476	2.4622	2.6058	2.5850	2.6180
RT Density (gm/cc)	1.2122	1.2113	1.2111	1.2107	1.2100	1.2109
T_g (°C,film)	139	145	150	154	156	161
T_g (°C, TBA)	138	145	152	154	156	

*Cure times at 161°C.

TABLE IVa

Summary of Data for XD7342/TMAB: Partially-Cured Systems (195°C)

Relative Humidity (%)	Equilibrium Moisture Gain (%) at 24.5°C					
	0.25 hr.*	0.5 hr.*	5 hr.*	24 hr.*	96 hr.*	240 hr.*
11	0.4749	0.5172	0.5558	0.6071	0.6328	0.6594
29	1.0504	1.1181	1.2307	1.3047	1.3749	1.4351
43	1.4919	1.5741	1.7428	1.8611	1.9460	2.0059
53	1.7831	1.8990	2.0871	2.2120	2.3179	2.3873
78	2.5907	2.7571	3.0198	3.2121	3.3868	3.5050
90	3.1249	3.3350	3.6363	3.8704	4.0562	4.2126
93	3.2392	3.4421	3.7904	3.9885	4.2106	4.3705
RT Density (gm/cc)	1.2596	1.2586	1.2586	1.2580	1.2566	1.2553
T_g (°C,TBA)	214	231.5	241	249	259	268.4

*Cure times at 195°C.

TABLE IVb

Summary of Data for XD7342/TMAB: Partially-Cured Systems (195°C)

Relative Humidity (%)	Equilibrium Moisture Gain (%) at 35.0°C					
	0.25 hr.*	0.5 hr.*	5 hr.*	24 hr.*	96 hr.*	240 hr.*
11	0.4074	0.4243	0.4650	0.5061	0.5652	0.5668
21	0.6979	0.7331	0.8054	0.8537	0.9317	0.9485
43	1.3492	1.4076	1.5403	1.6339	1.7404	1.8088
50	1.5384	1.6251	1.7658	1.8544	2.0031	2.1041
75	2.3941	2.5288	1.7168	2.8298	3.0488	3.1951
89.5	2.9673	3.1071	3.3749	3.5430	3.7477	3.8947
91.5	3.0259	3.1692	3.4611	3.5381	3.8608	3.9649

*Cure times at 195°C.

TABLE V

Dual Mode Sorption Parameters

DER337/TMAB (161°C Cure)

Cure Time (hr) at 161°C	k_D[cm^3(STP)/cm^3-cm Hg]	C_H'[cm^3(STP)/cm^3]	b[cm Hg^{-1}]
3	10	6.3	1.3
5	13	1.6	32
11	14	2.7	8.0
29	15	2.5	9.7
72	15	2.7	6.8
341	14	3.1	5.2
*	12.6	15	1.2

*data from ref. 34

TABLE VI

Dual Mode Sorption Parameters: XD7342/TMAB (195°C, 24 hr. Cure)

Temperature (°C)	k_D [cm³(STP)/cm³-cmHg]	C_H' [cm³(STP)/cm³]	b[cmHg^{-1}]
24.5	25.3	4.13	11.4
35.0	12.8	2.37	10.9
45.0 (Experimental)	7.77	1.57	4.60
45.0 (Predicted)	6.91	1.45	10.5

TABLE VII

Comparison of Studies of Extent of Cure on Properties of Epoxy Resins

Property \ System	DER337/TMAB[a] XD/TMAB[a]	TGDDM/DDS[b]	TGDDM/DDS[c]	Epon 828/m-PD/aniline[d]
T_g	·	·	·	·
RT M_x	·	·	.	·
RT ρ	.	-	-	·
RT D	.	-	.	·

Key: · = increases as extent of cure increases
. = decreases as extent of cure increases
- = not reported

a present study
b ref. 61
c ref. 33
d ref. 5

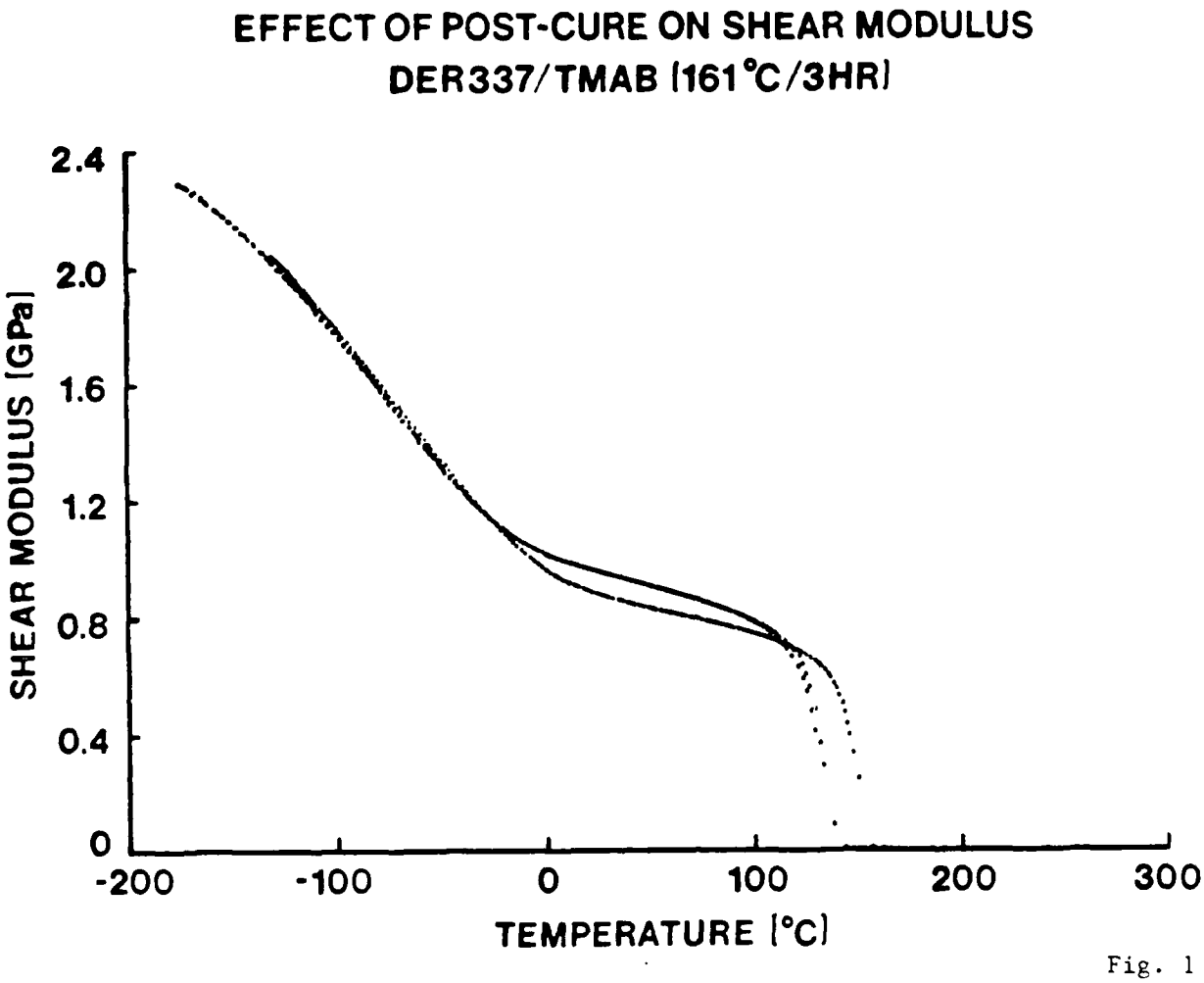
EFFECT OF POST-CURE ON SHEAR MODULUS
DER337/TMAB [161°C/3HR]
SHEAR MODULUS [GPa]
2.4
2.0
1.6
1.2
0.8
0.4
0
-200
-100
0
100
200
300
TEMPERATURE [°C]

Fig. 1

CHEMICAL FORMULAE

Diglycidyl Ether of Bisphenol A (DER337)

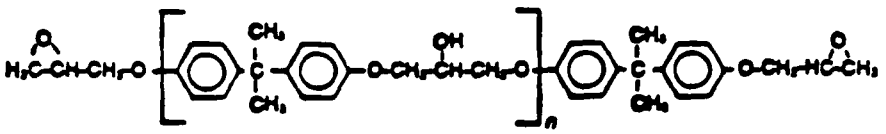

Triglycidyl Ether of Tris (Hydroxyphenyl) Methane (XD7342)

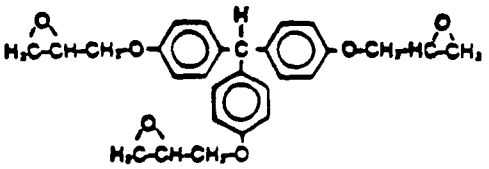

Trimethylene Glycol Di-p-aminobenzoate (TMAB)

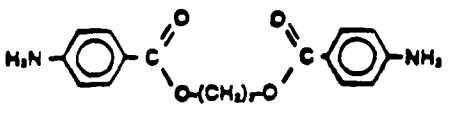

Fig. 2

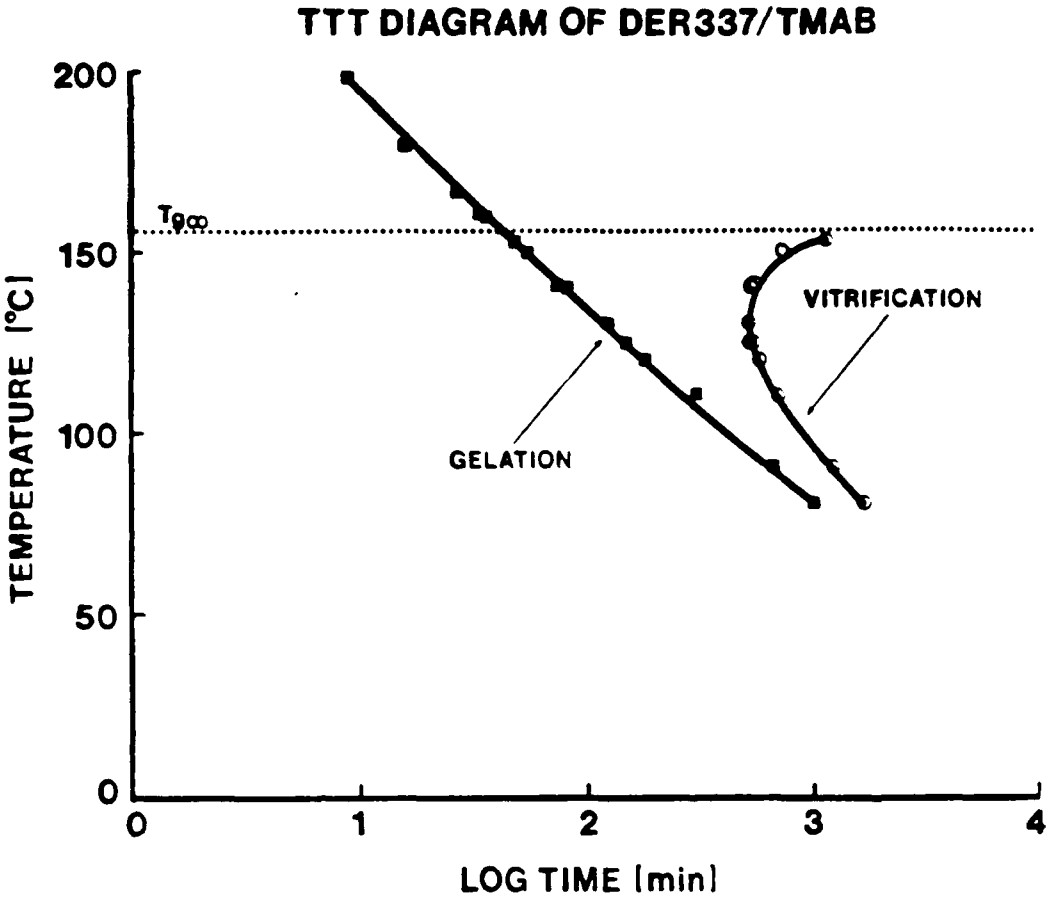
TTT DIAGRAM OF DER337/TMAB
200
150
100
50
0
$T_{g\infty}$
TEMPERATURE [°C]
VITRIFICATION
GELATION
0
1
2
3
4
LOG TIME [min]

Fig. 3a

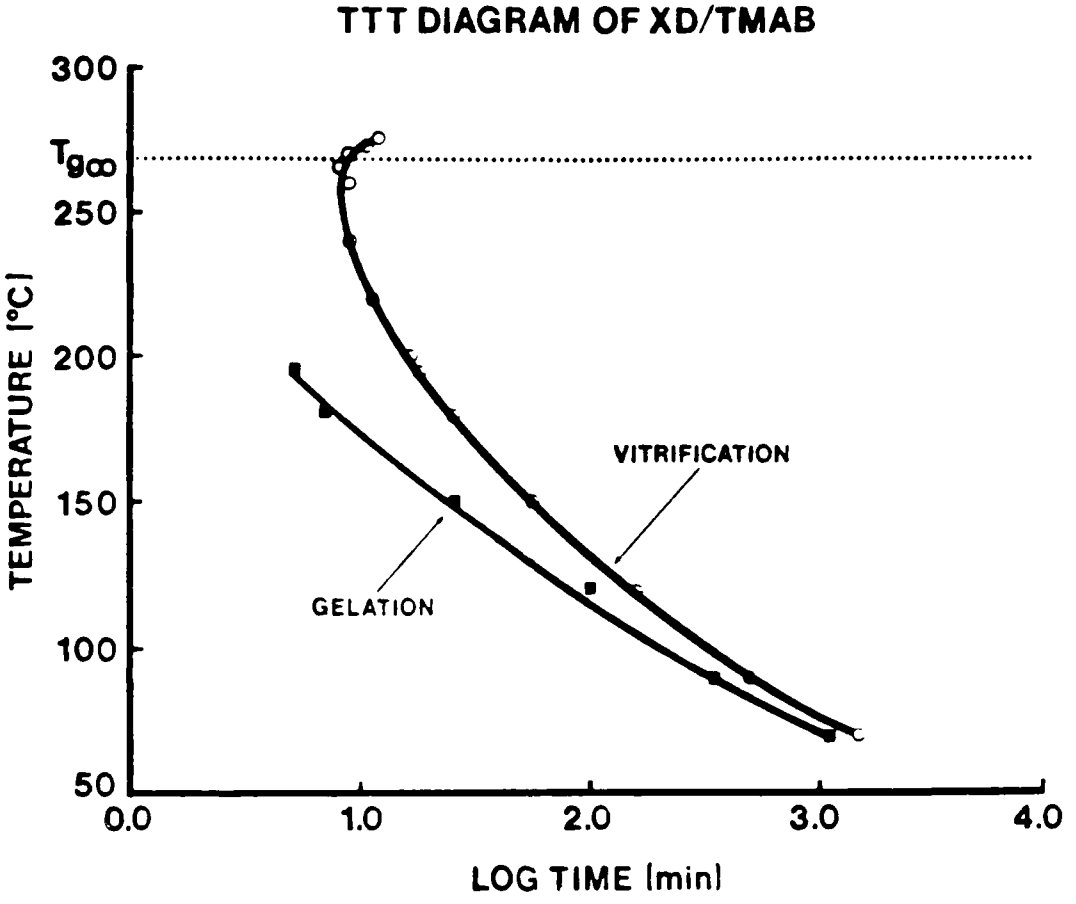
TTT DIAGRAM OF XD/TMAB
300
$T_{g\infty}$
250
200
150
100
50
TEMPERATURE (°C)
VITRIFICATION
GELATION
0.0
1.0
2.0
3.0
4.0
LOG TIME (min)

Fig. 3b

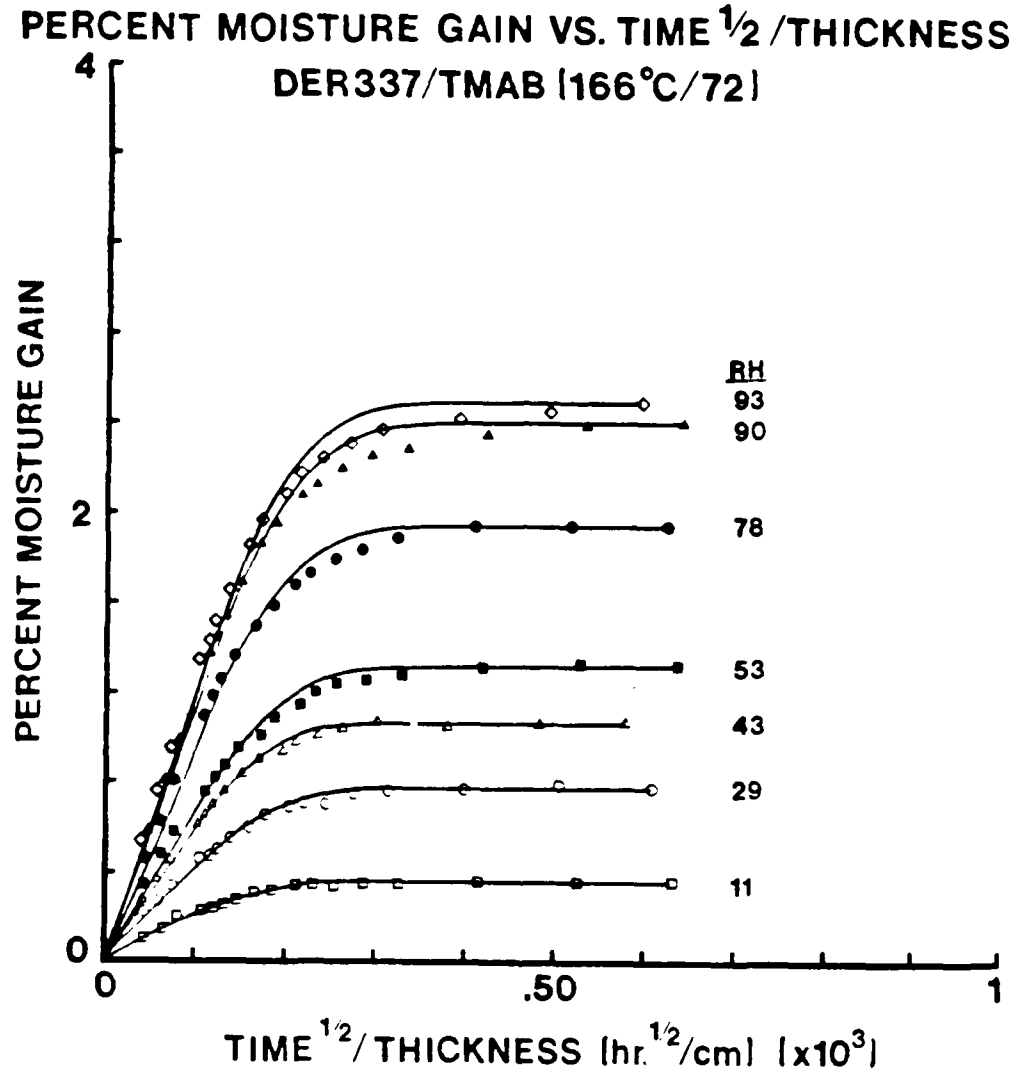
PERCENT MOISTURE GAIN VS. TIME 1/2 /THICKNESS
DER337/TMAB [166°C/72]
PERCENT MOISTURE GAIN
4
2
0
0
.50
1
TIME 1/2/ THICKNESS [hr.1/2/cm] [x10³]
RH
93
90
78
53
43
29
11

Fig. 4

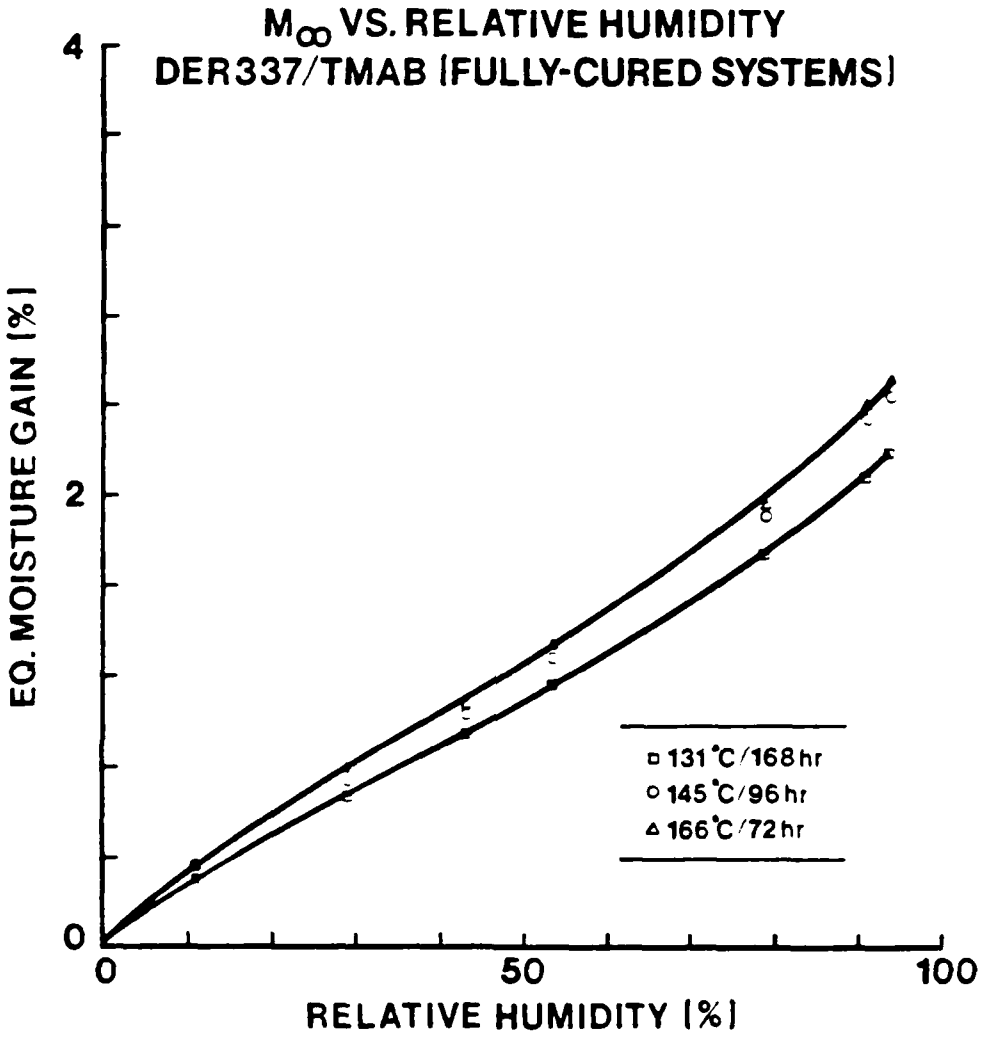
M_∞ VS. RELATIVE HUMIDITY
DER337/TMAB (FULLY-CURED SYSTEMS)
EQ. MOISTURE GAIN (%)
4
2
0
0
50
100
RELATIVE HUMIDITY (%)
□ 131°C/168hr
○ 145°C/96hr
△ 166°C/72hr

Fig. 5

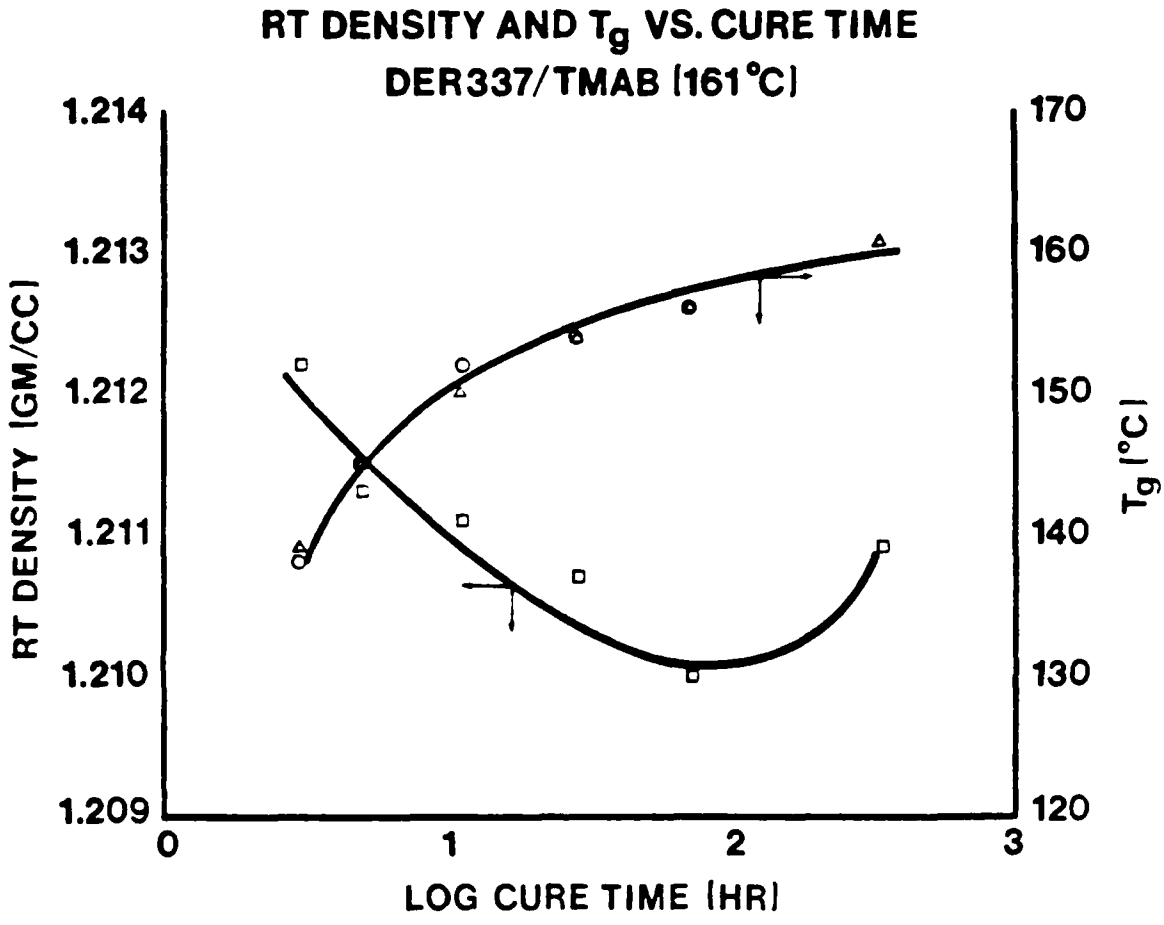
RT DENSITY AND T_g VS. CURE TIME
DER337/TMAB (161°C)
1.214
1.213
1.212
1.211
1.210
1.209
RT DENSITY (GM/CC)
170
160
150
140
130
120
T_g (°C)
0
1
2
3
LOG CURE TIME (HR)

Fig. 6

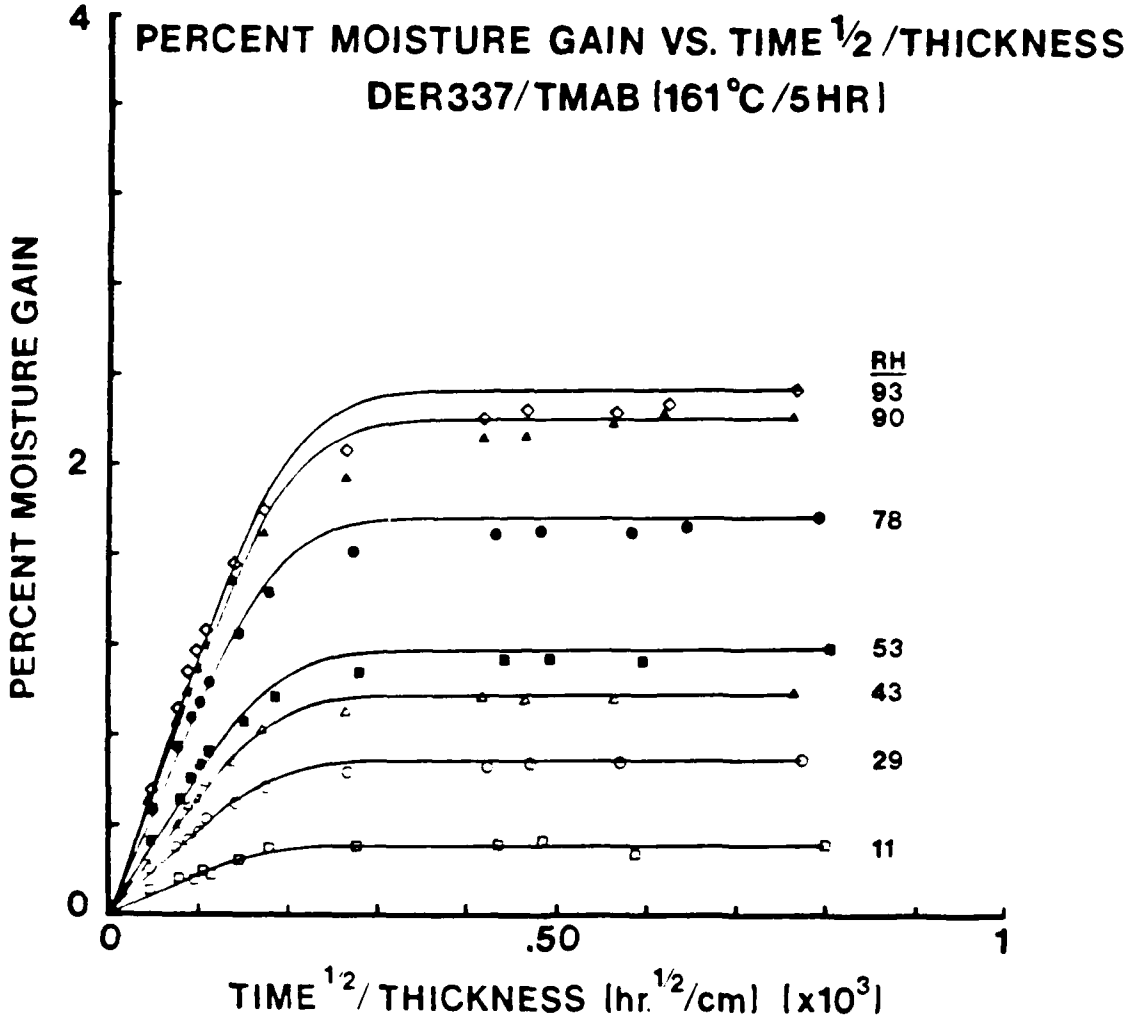
PERCENT MOISTURE GAIN VS. TIME 1/2 /THICKNESS
DER337/TMAB [161°C/5HR]
PERCENT MOISTURE GAIN
4
2
0
0
.50
1
TIME 1/2 / THICKNESS [hr. 1/2/cm] [x10 3]
RH
93
90
78
53
43
29
11

Fig. 7

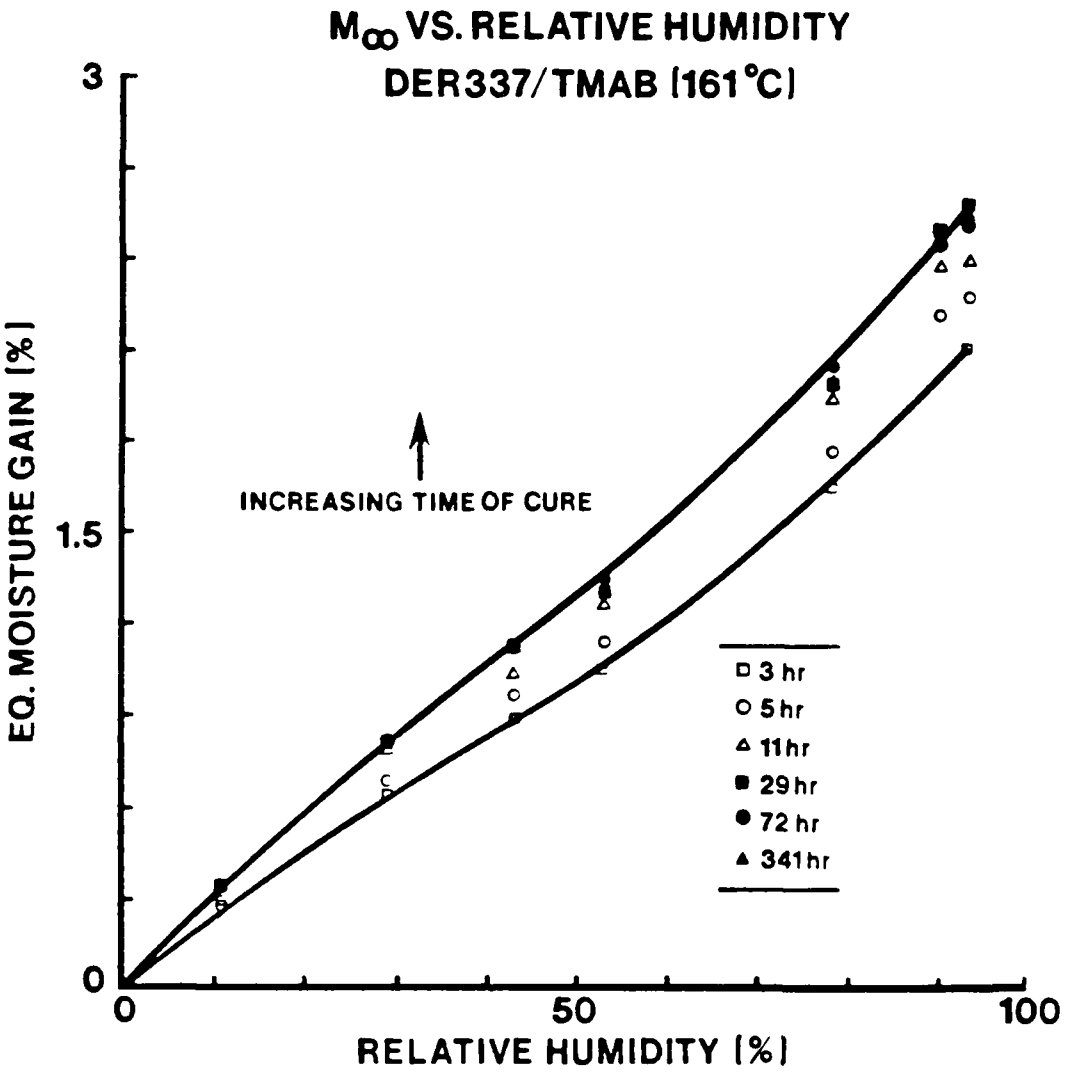
M_∞ VS. RELATIVE HUMIDITY
DER337/TMAB (161°C)
EQ. MOISTURE GAIN (%)
3
1.5
0
INCREASING TIME OF CURE
3 hr
5 hr
11 hr
29 hr
72 hr
341 hr
0
50
100
RELATIVE HUMIDITY (%)

Fig. 8

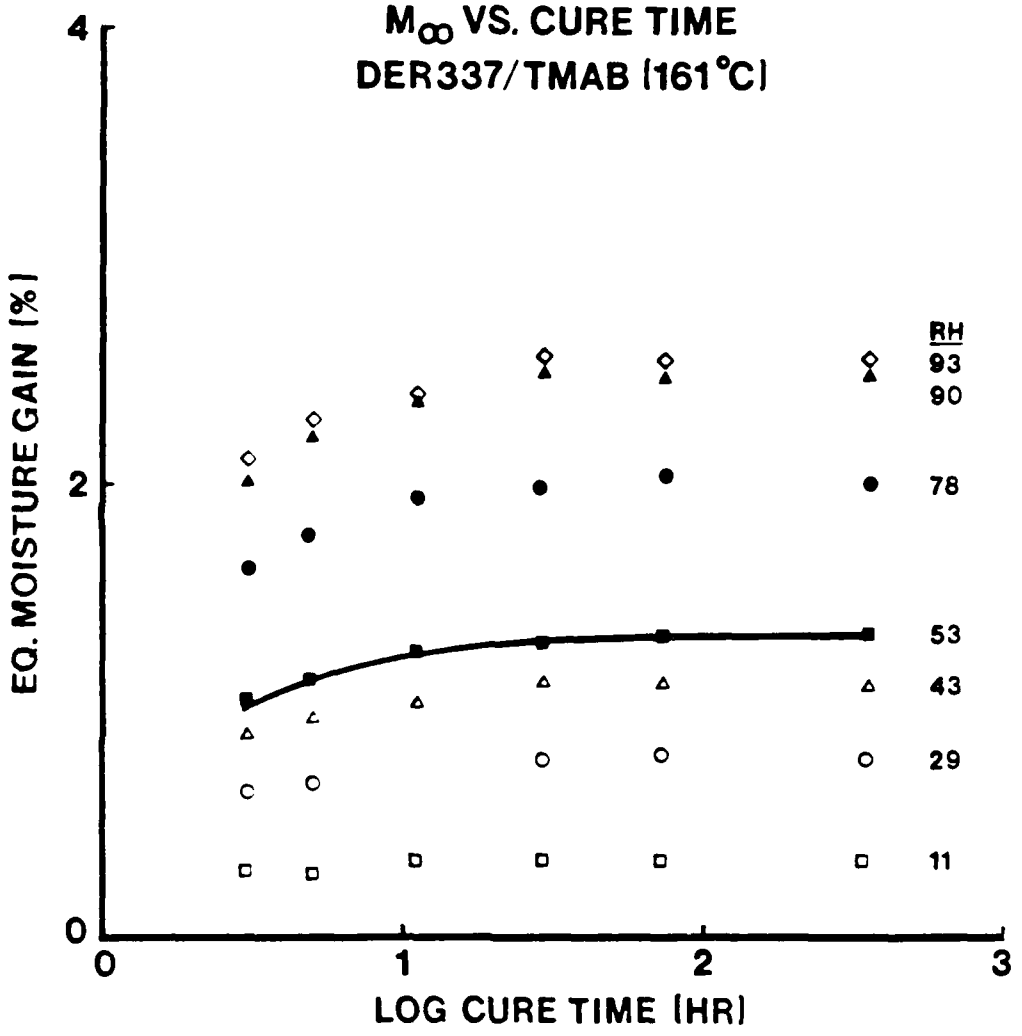
M_∞ VS. CURE TIME
DER337/TMAB (161°C)
EQ. MOISTURE GAIN (%)
LOG CURE TIME (HR)
RH
93
90
78
53
43
29
11
0
1
2
3
4

Fig. 9

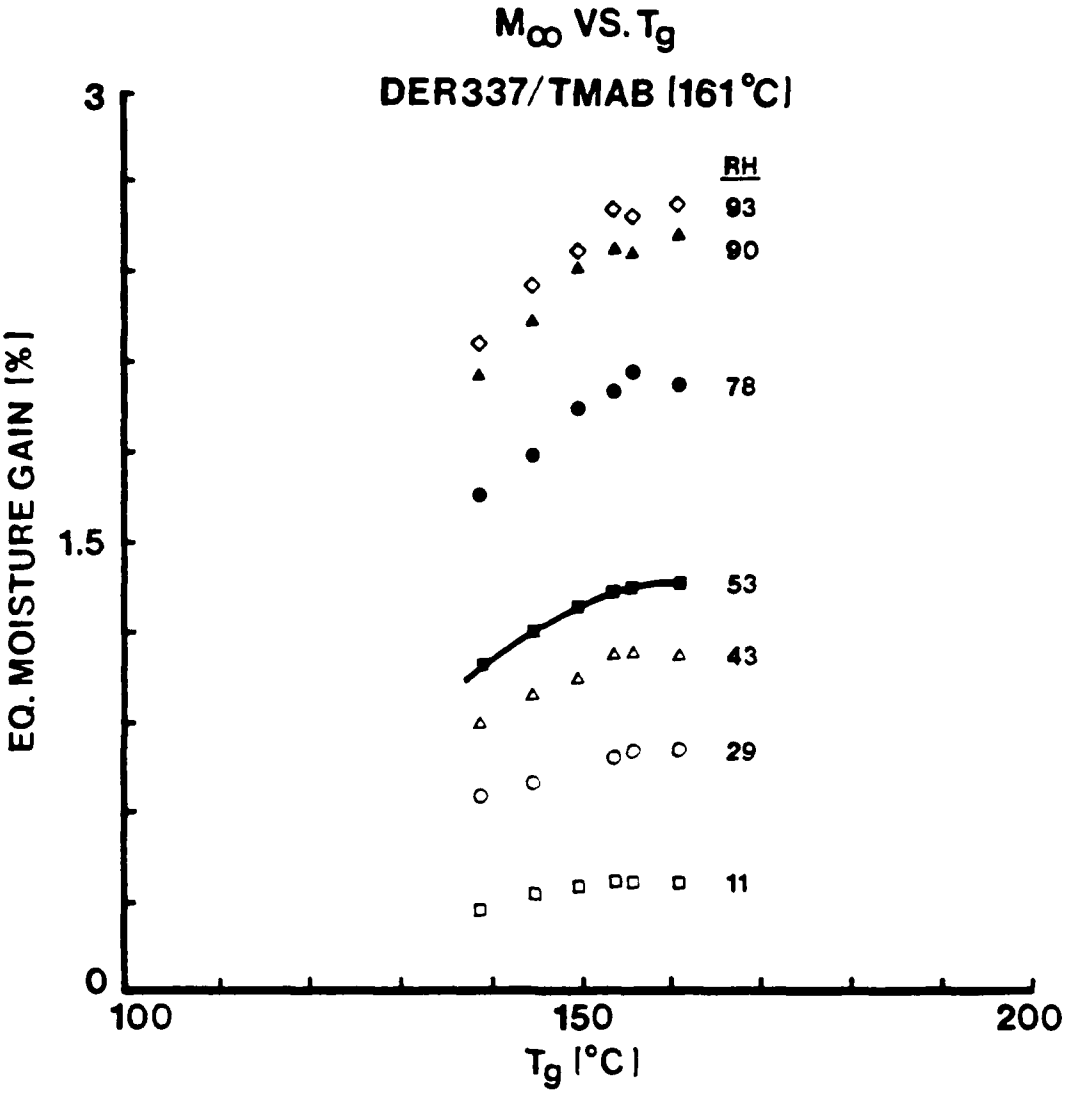
M_∞ VS. T_g
DER337/TMAB (161°C)
RH
93
90
78
53
43
29
11
EQ. MOISTURE GAIN (%)
3
1.5
0
100
150
200
T_g (°C)

Fig. 10

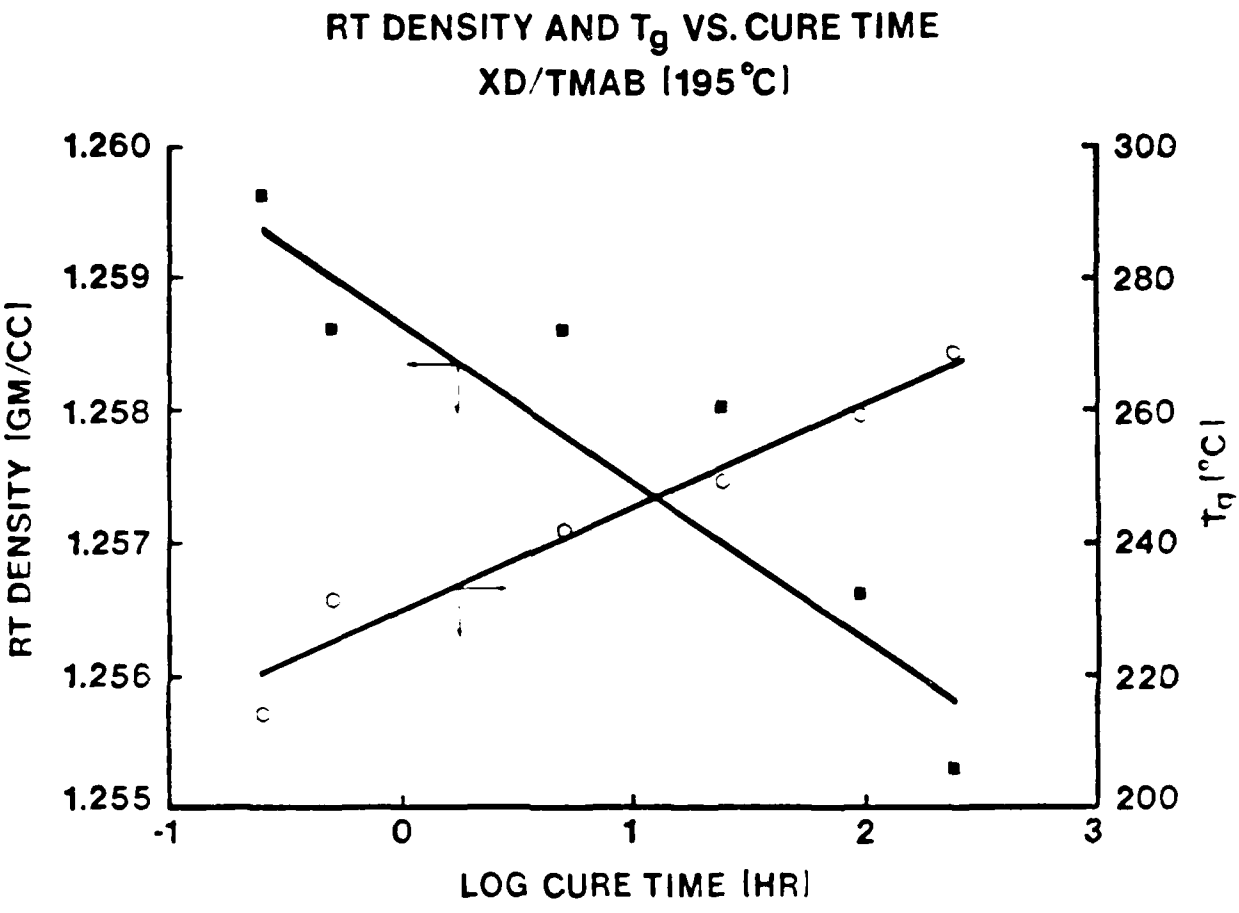
RT DENSITY AND T_g VS. CURE TIME
XD/TMAB (195°C)
1.260
1.259
1.258
1.257
1.256
1.255
RT DENSITY (GM/CC)
300
280
260
240
220
200
T_g (°C)
-1
0
1
2
3
LOG CURE TIME (HR)

Fig. 11

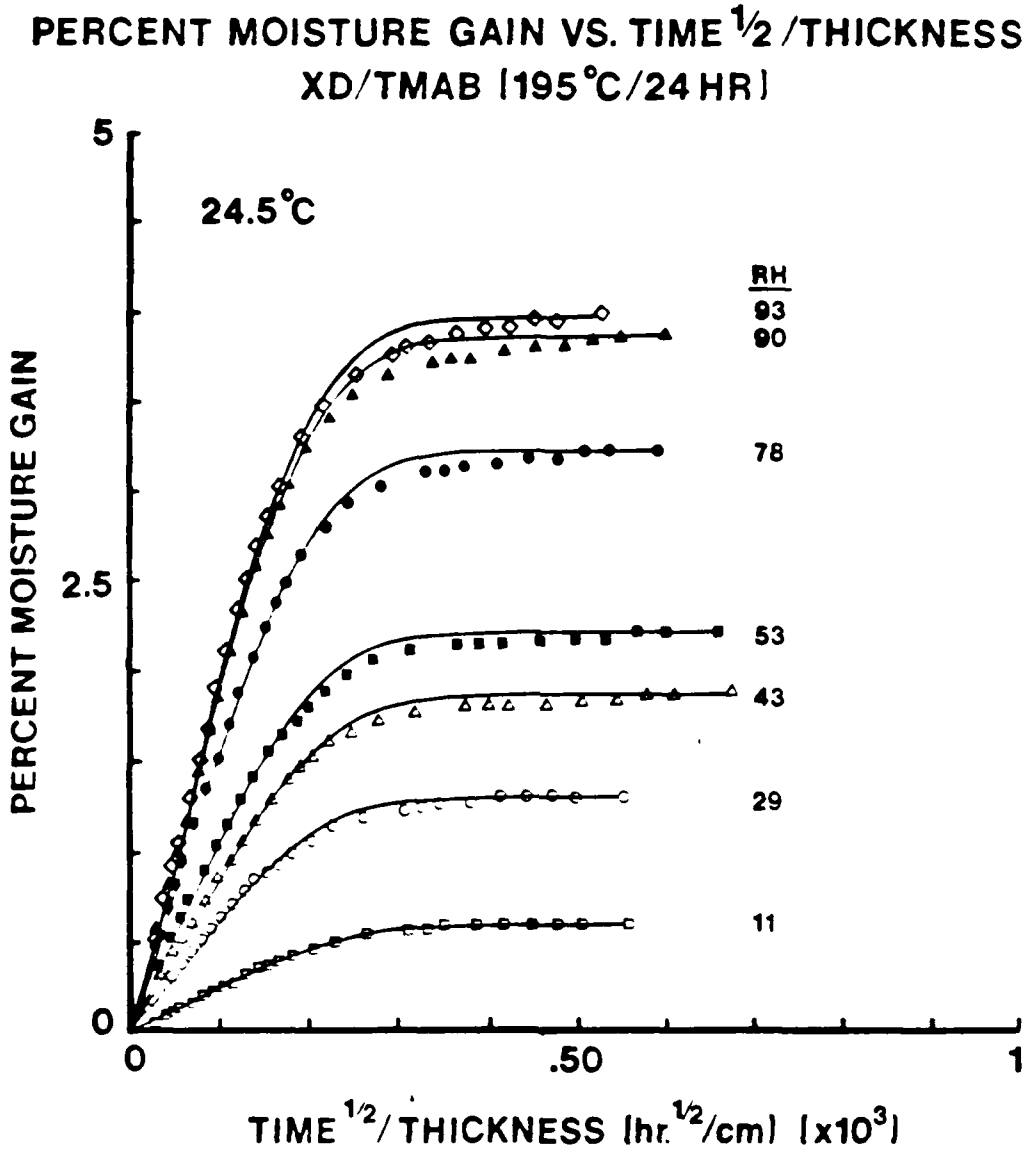
PERCENT MOISTURE GAIN VS. TIME 1/2 /THICKNESS
XD/TMAB [195°C/24 HR]
24.5°C
RH
93
90
78
53
43
29
11
PERCENT MOISTURE GAIN
5
2.5
0
0
.50
1
TIME 1/2 / THICKNESS [hr. 1/2/cm] [x10³]

Fig. 12a

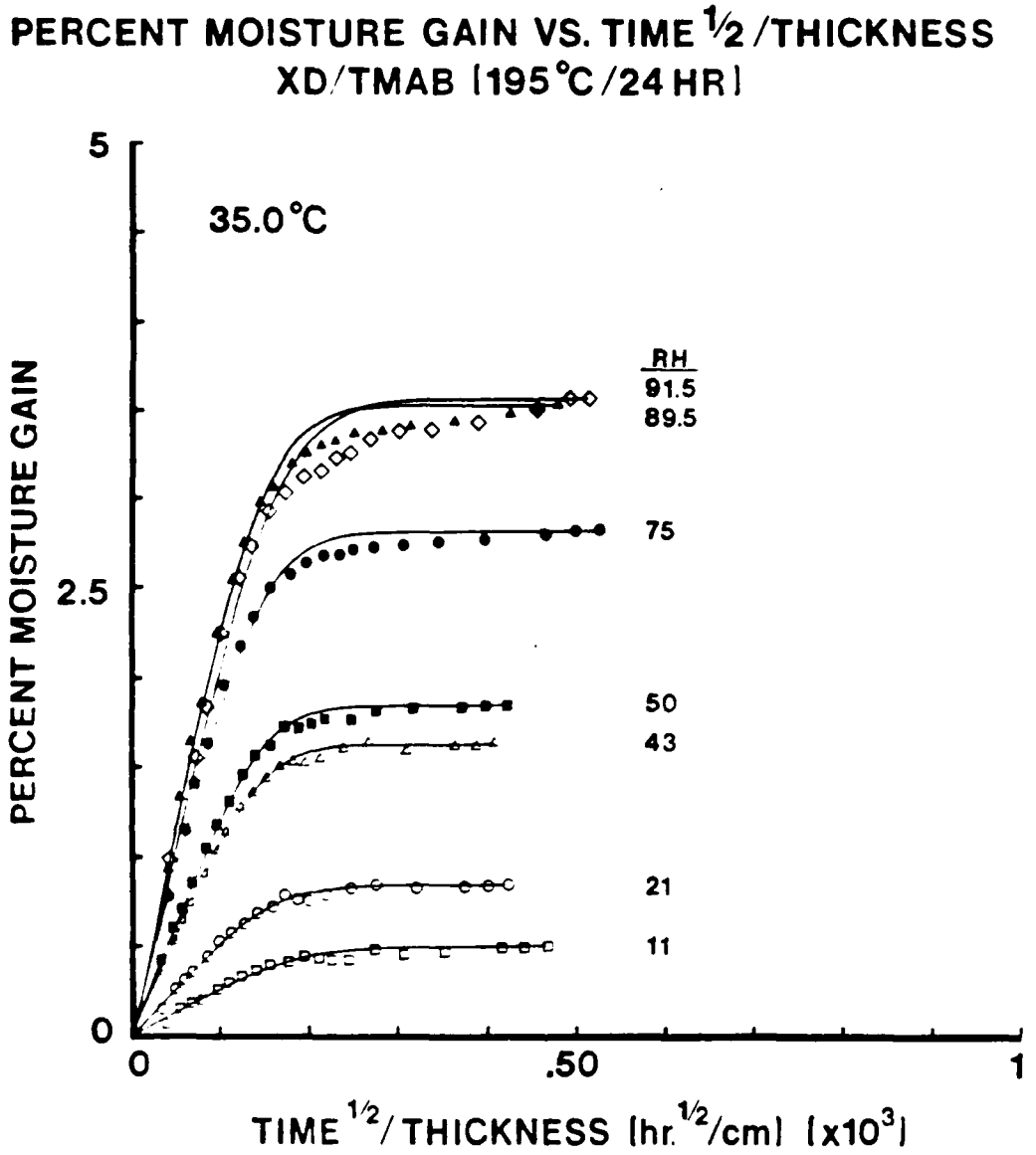
PERCENT MOISTURE GAIN VS. TIME 1/2 /THICKNESS
XD/TMAB [195°C/24 HR]
35.0°C
RH
91.5
89.5
75
50
43
21
11
PERCENT MOISTURE GAIN
5
2.5
0
0
.50
1
TIME 1/2 / THICKNESS [hr. 1/2 /cm] [x10 3]

Fig. 12b

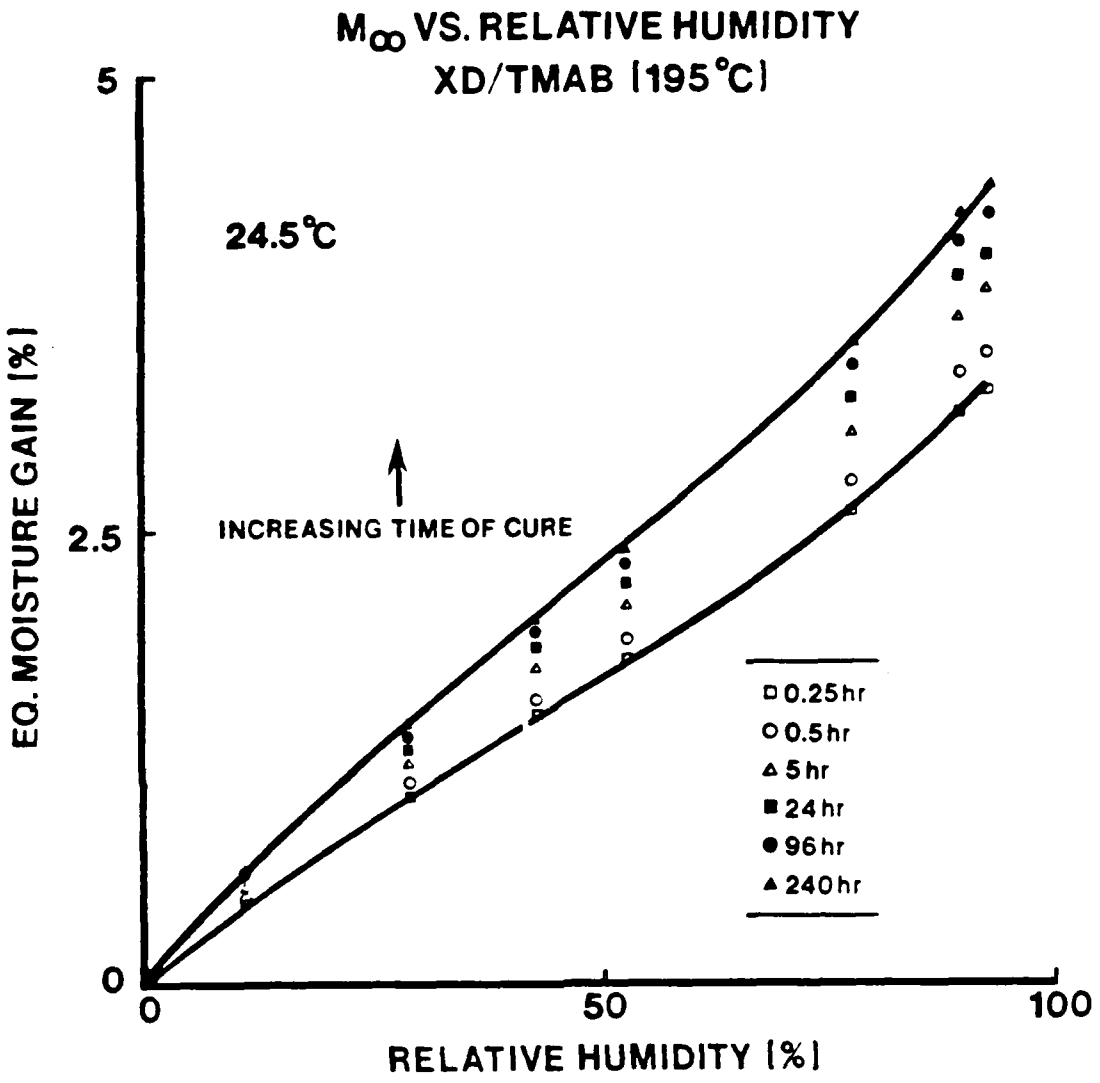
M_∞ VS. RELATIVE HUMIDITY
XD/TMAB [195°C]
24.5°C
INCREASING TIME OF CURE
EQ. MOISTURE GAIN [%]
RELATIVE HUMIDITY [%]
5
2.5
0
0
50
100
0.25hr
0.5hr
5hr
24hr
96hr
240hr

Fig. 13a

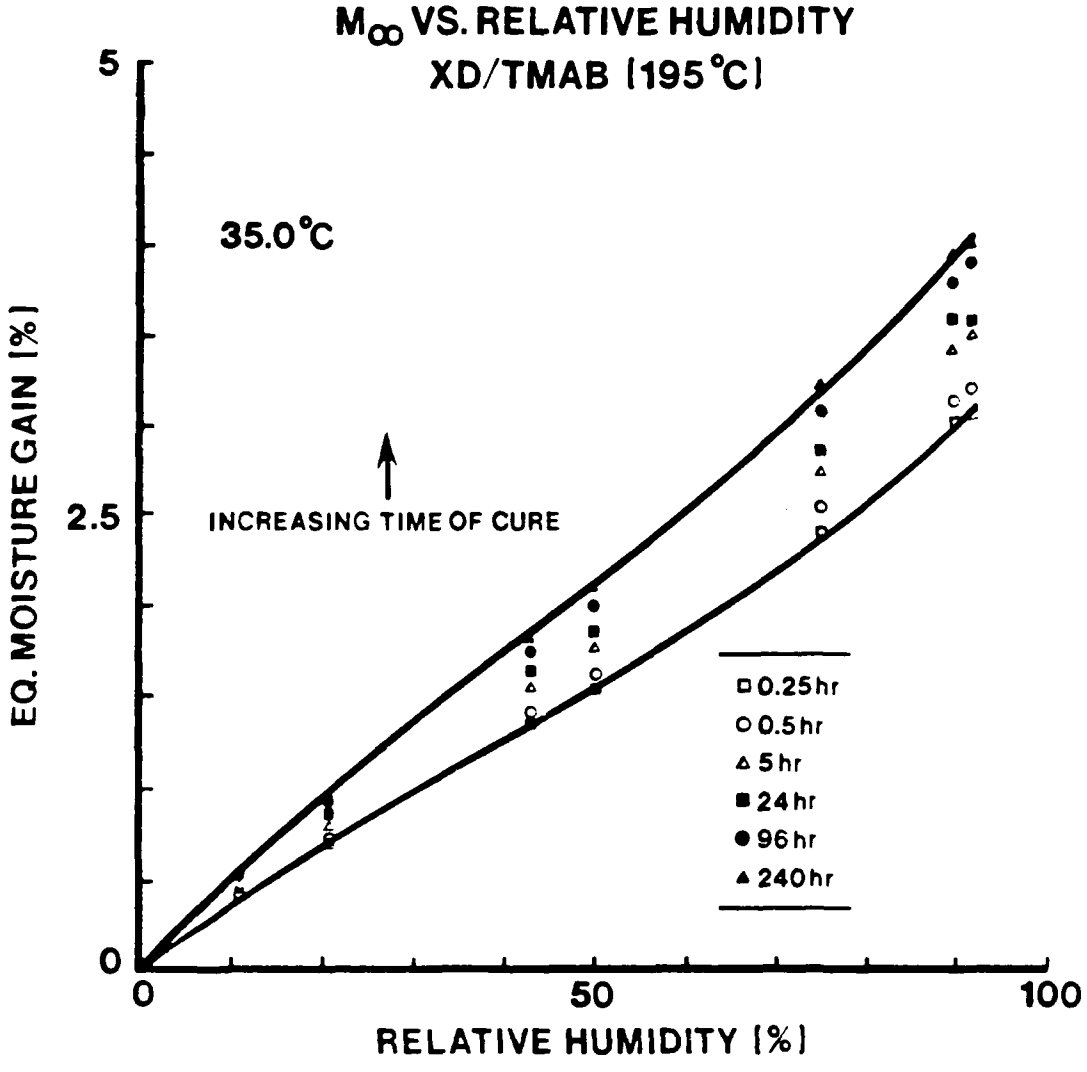
M_∞ VS. RELATIVE HUMIDITY
XD/TMAB (195°C)
35.0°C
INCREASING TIME OF CURE
EQ. MOISTURE GAIN (%)
RELATIVE HUMIDITY (%)
0
2.5
5
0
50
100
0.25hr
0.5hr
5hr
24hr
96hr
240hr

Fig. 13b

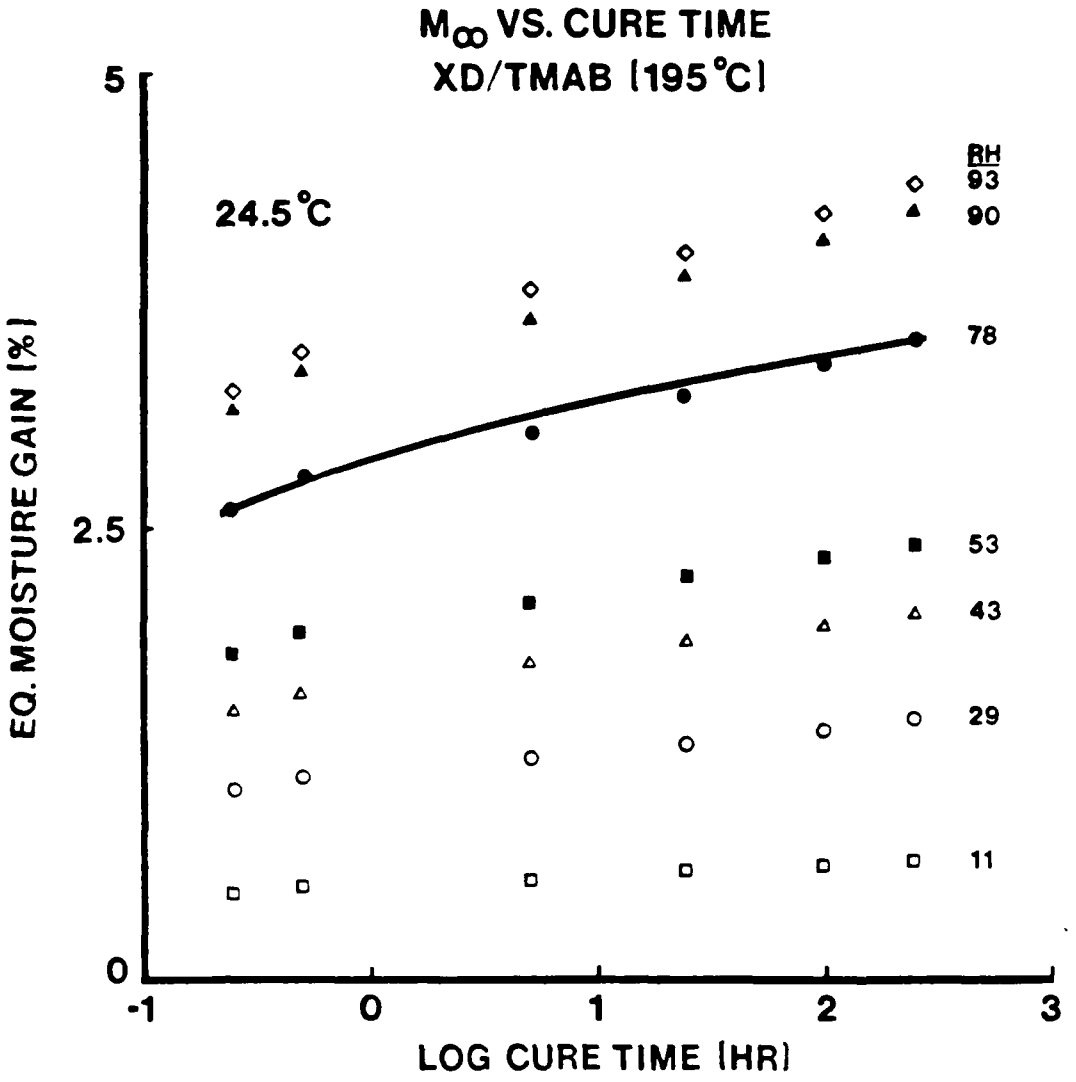
M_∞ VS. CURE TIME
XD/TMAB (195°C)
24.5°C
RH
93
90
78
53
43
29
11
EQ. MOISTURE GAIN (%)
5
2.5
0
-1
0
1
2
3
LOG CURE TIME (HR)

Fig. 14a

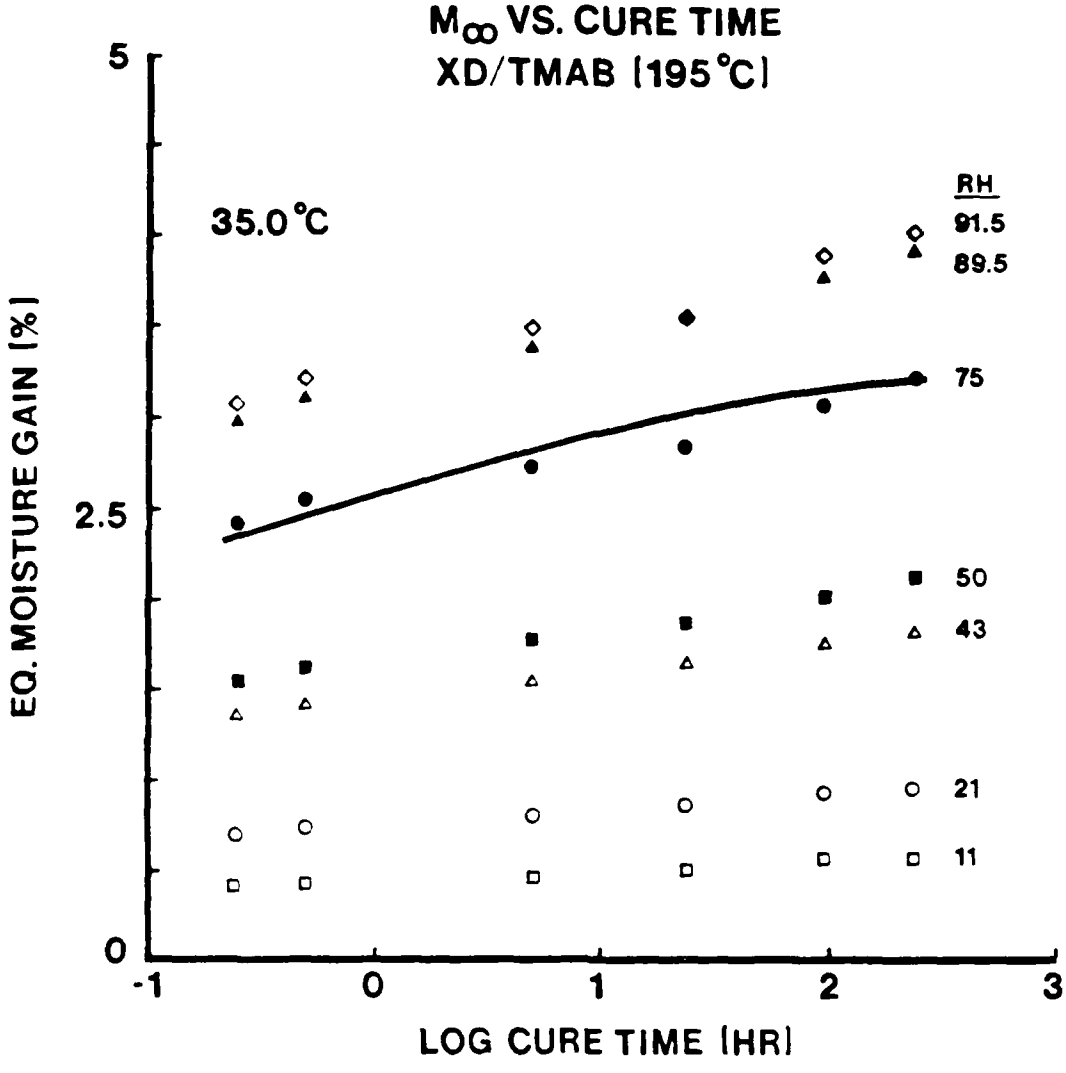
M_∞ VS. CURE TIME
XD/TMAB (195°C)
35.0°C
RH
91.5
89.5
75
50
43
21
11
EQ. MOISTURE GAIN (%)
5
2.5
0
-1
0
1
2
3
LOG CURE TIME (HR)

Fig. 14b

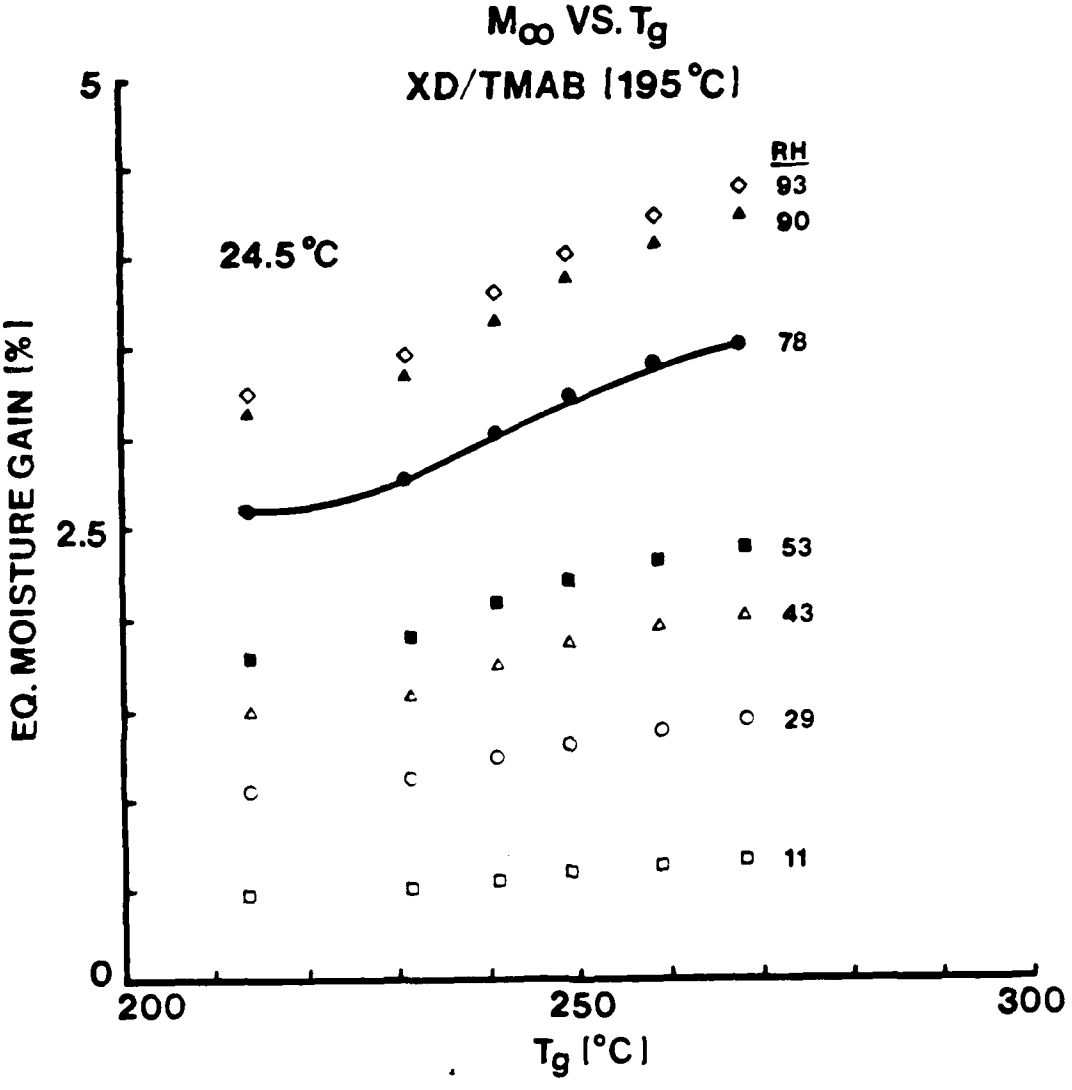
M_∞ VS. T_g
XD/TMAB (195°C)
RH
93
90
78
53
43
29
11
24.5°C
EQ. MOISTURE GAIN (%)
5
2.5
0
200
250
300
T_g (°C)

Fig. 15a

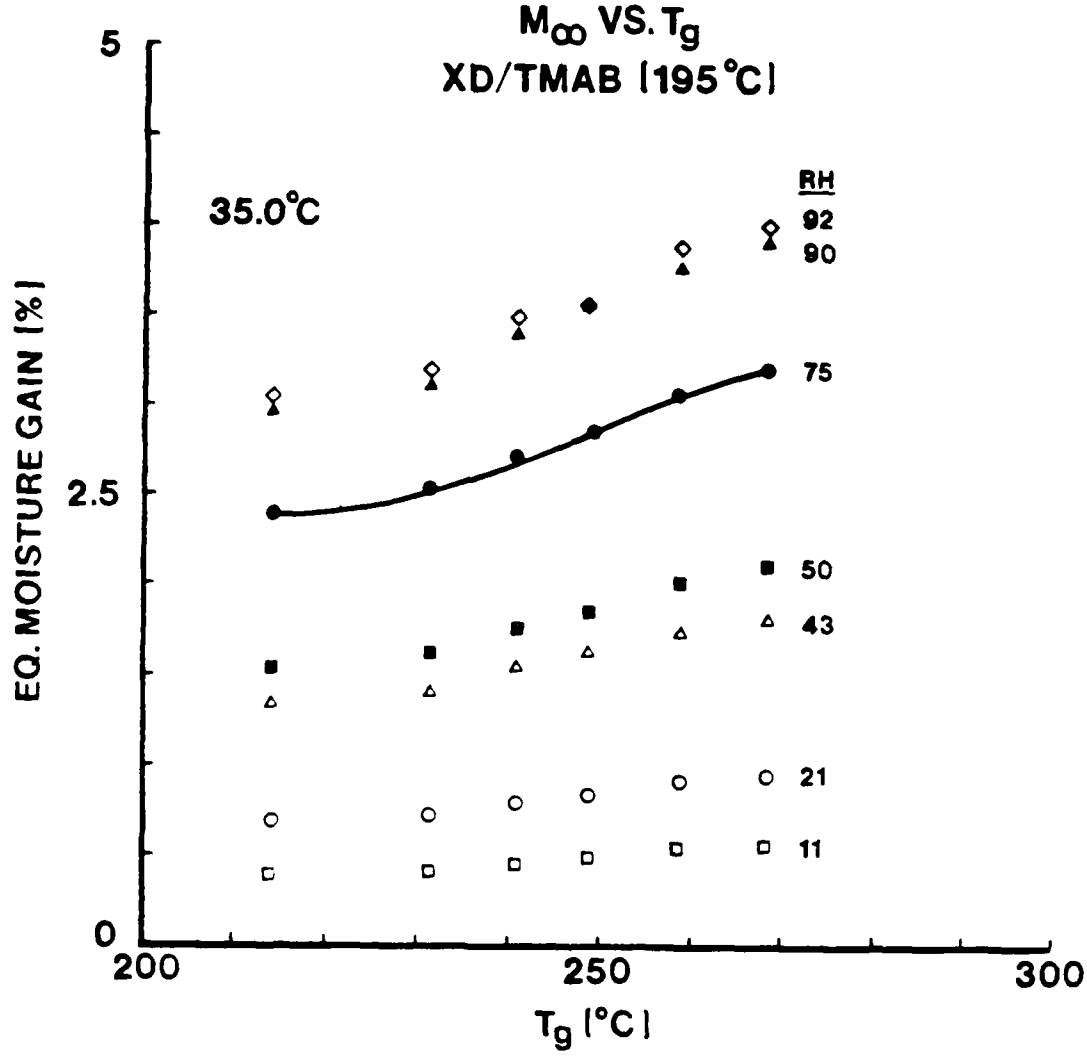
M_∞ VS. T_g
XD/TMAB (195°C)
35.0°C
RH
92
90
75
50
43
21
11
EQ. MOISTURE GAIN (%)
5
2.5
0
200
250
300
T_g (°C)

Fig. 15b

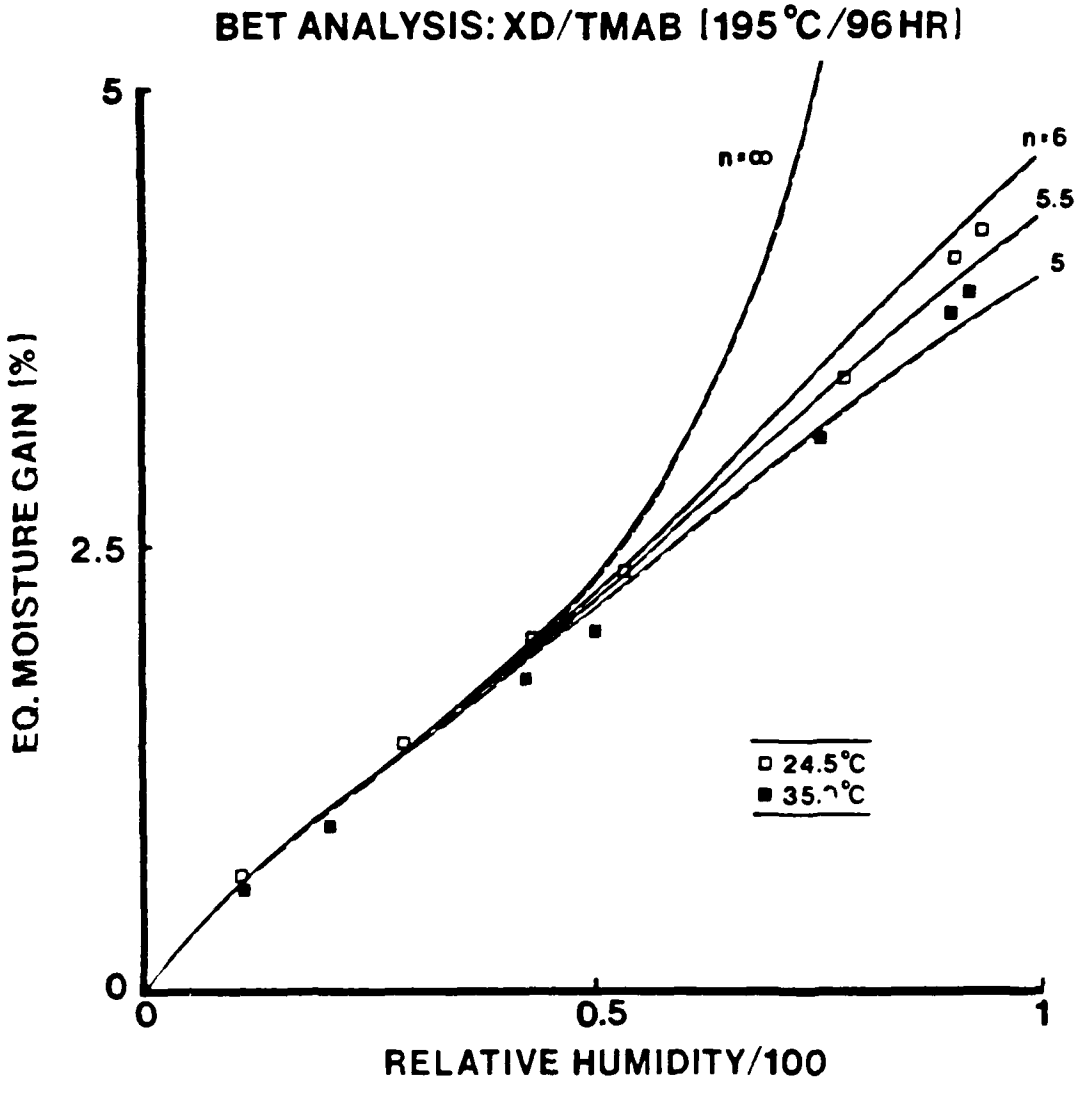
BET ANALYSIS: XD/TMAB [195°C/96HR]
EQ. MOISTURE GAIN [%]
5
2.5
0
0
0.5
1
RELATIVE HUMIDITY/100
n=∞
n=6
5.5
5
□ 24.5°C
■ 35.0°C

Fig. 16

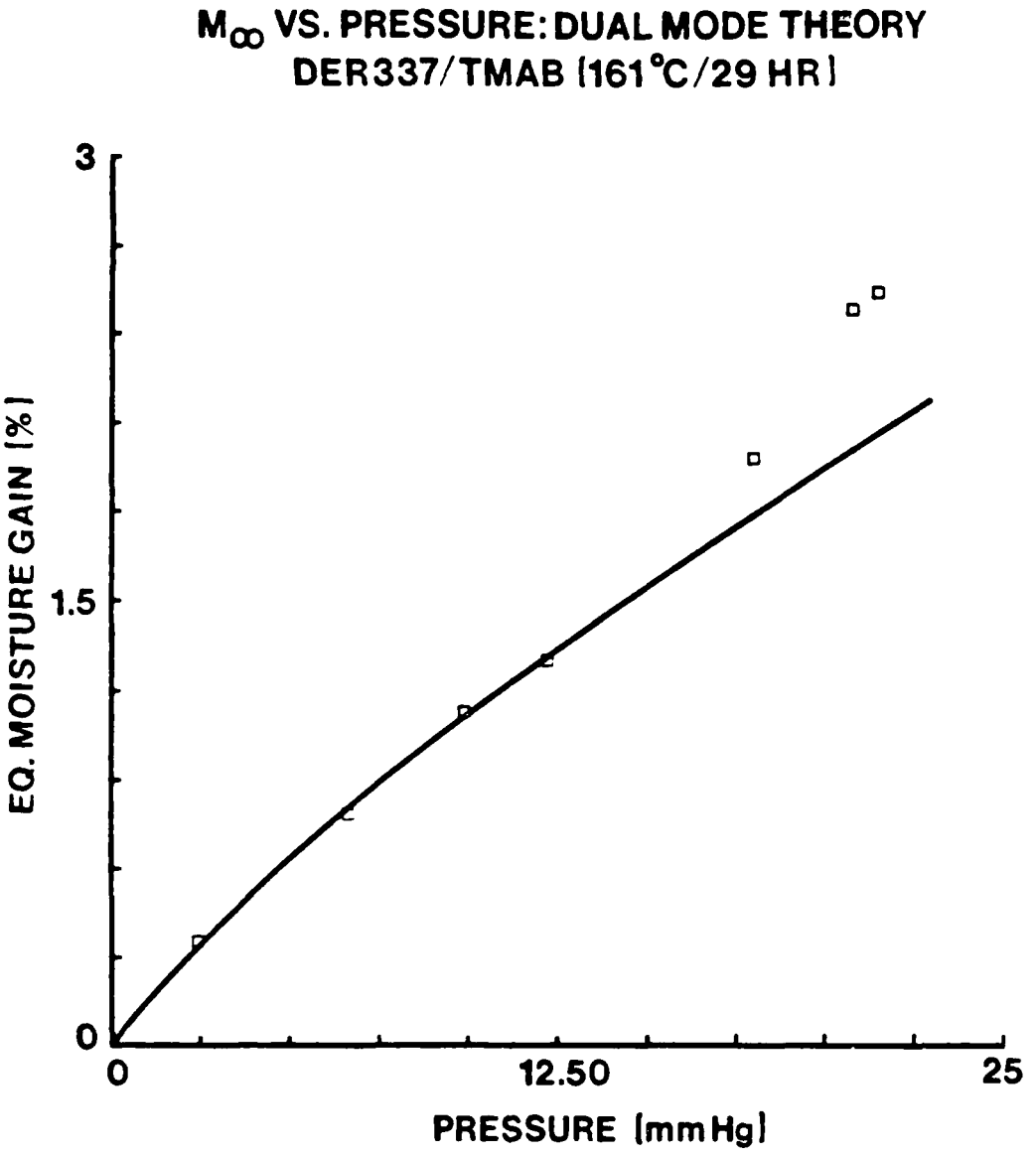
M_∞ VS. PRESSURE: DUAL MODE THEORY
DER337/TMAB (161°C/29 HR)
EQ. MOISTURE GAIN (%)
3
1.5
0
0
12.50
25
PRESSURE (mmHg)

Fig. 17

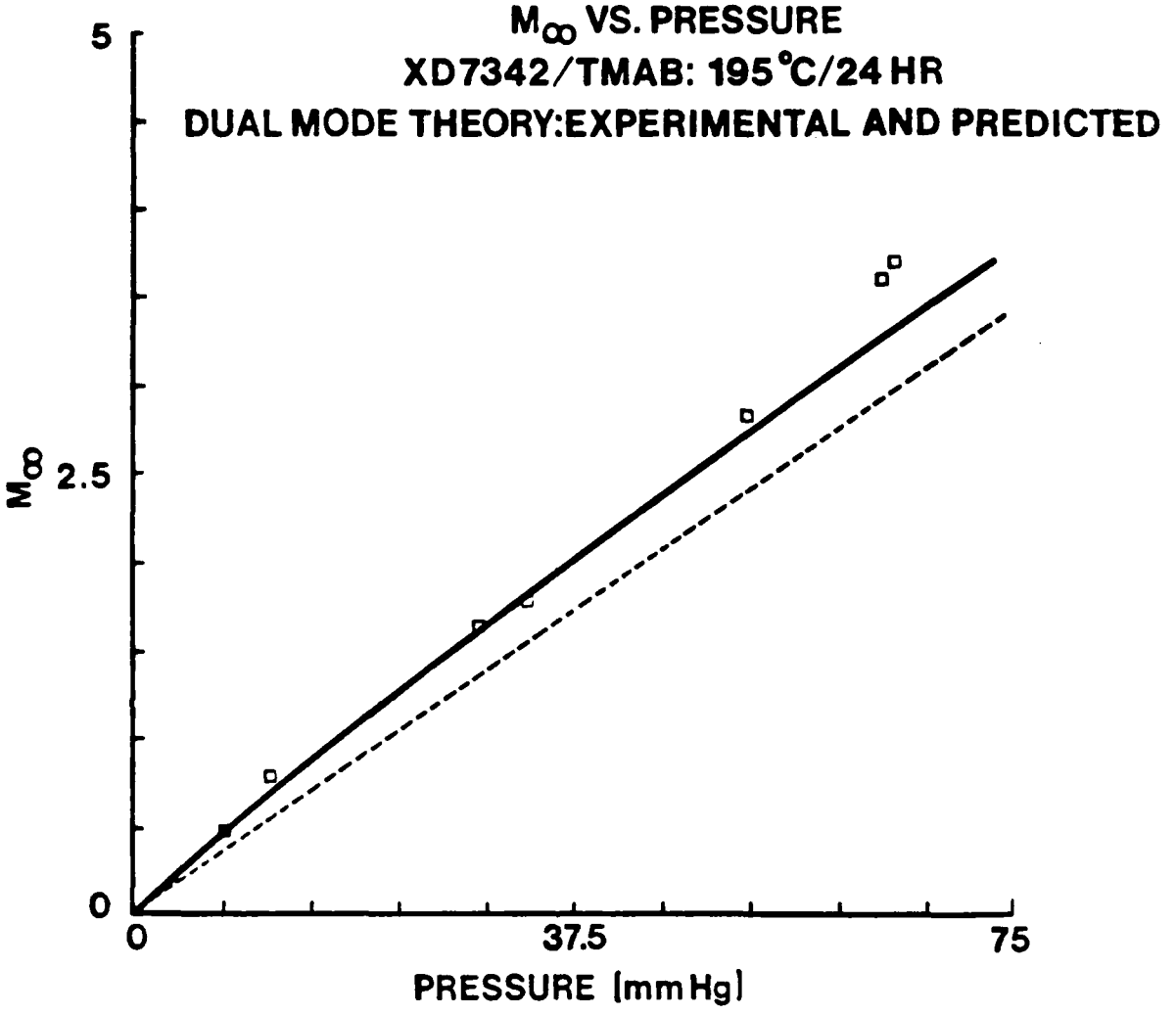
M_∞ VS. PRESSURE
XD7342/TMAB: 195°C/24 HR
DUAL MODE THEORY:EXPERIMENTAL AND PREDICTED
5
2.5
0
M_∞
0
37.5
75
PRESSURE (mmHg)

Fig. 18

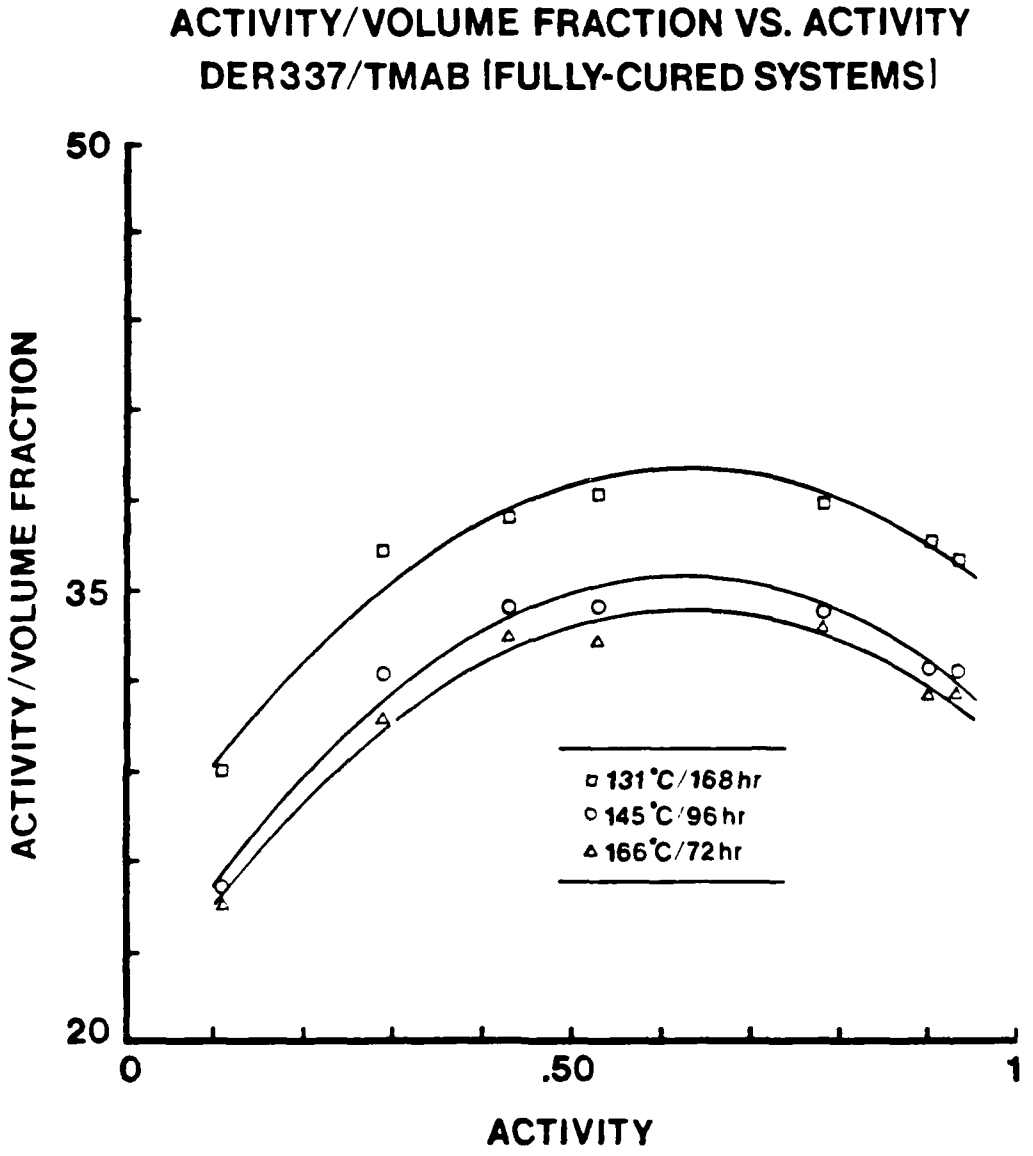
ACTIVITY/VOLUME FRACTION VS. ACTIVITY
DER337/TMAB (FULLY-CURED SYSTEMS)
50
35
20
ACTIVITY/VOLUME FRACTION
0
.50
1
ACTIVITY
131°C/168hr
145°C/96hr
166°C/72hr

Fig. 19

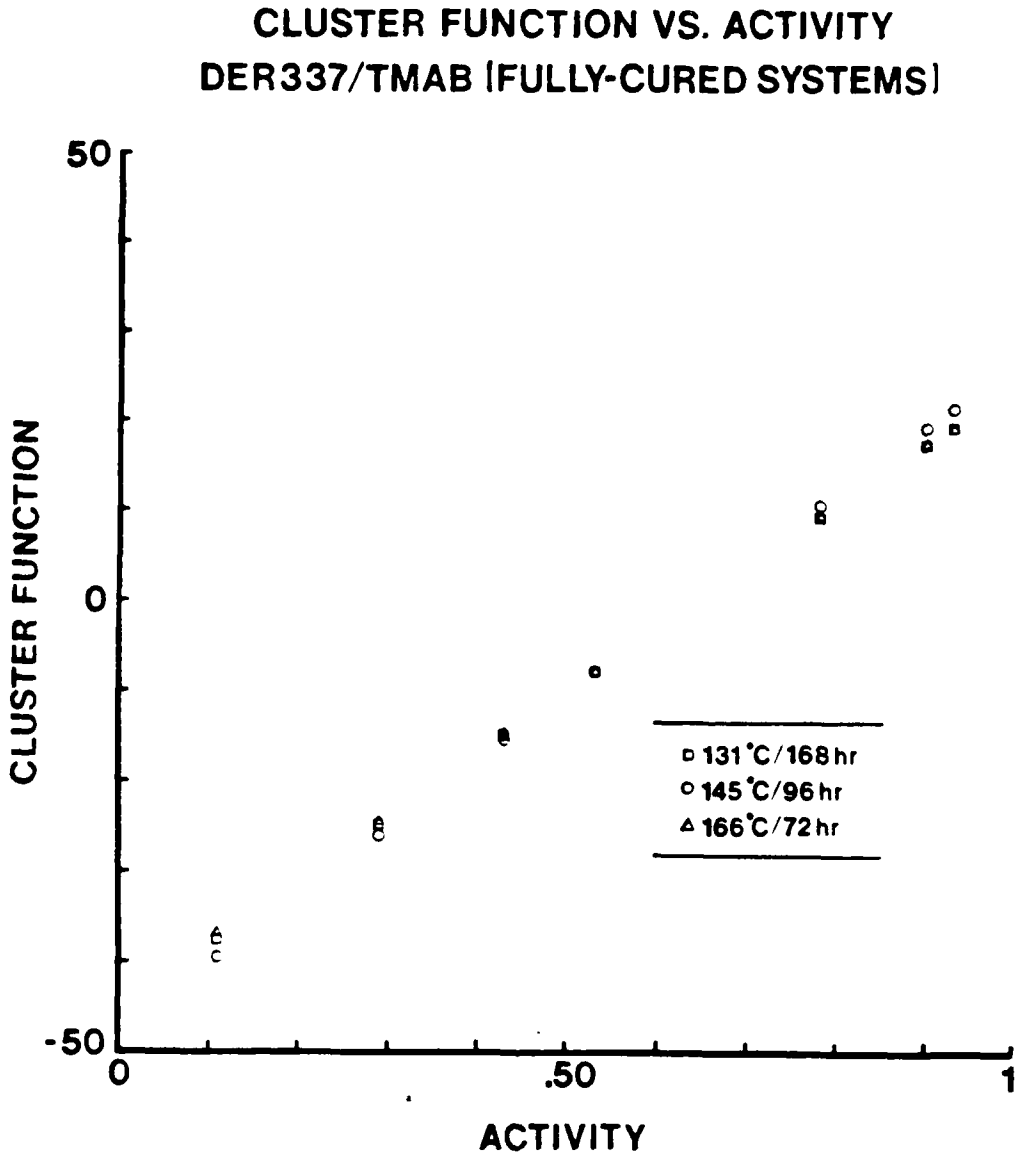
CLUSTER FUNCTION VS. ACTIVITY
DER337/TMAB [FULLY-CURED SYSTEMS]
50
0
-50
CLUSTER FUNCTION
0
.50
1
ACTIVITY
131°C/168hr
145°C/96hr
166°C/72hr

Fig. 20

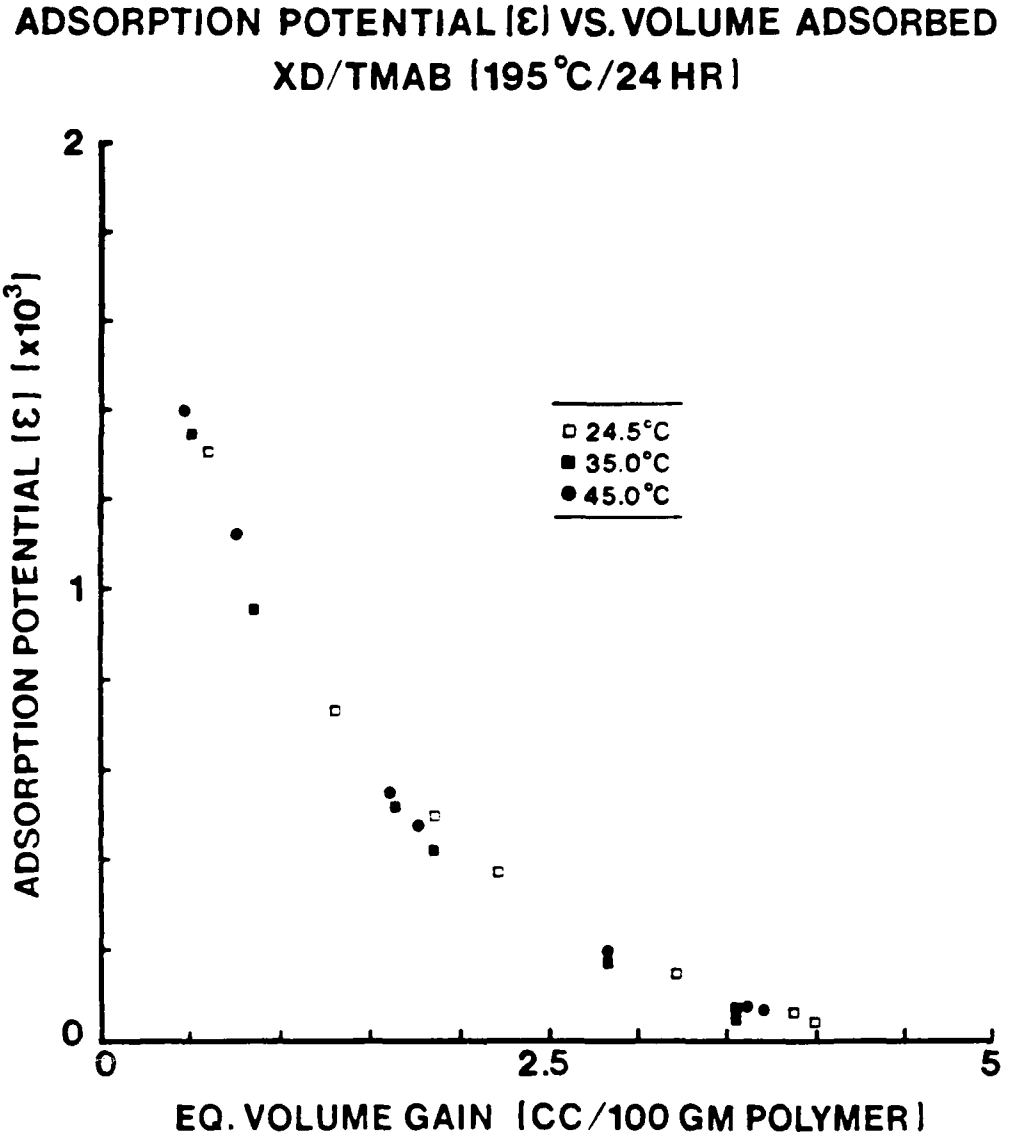
ADSORPTION POTENTIAL [ε] VS. VOLUME ADSORBED
XD/TMAB [195°C/24 HR]
ADSORPTION POTENTIAL [ε] [x10³]
2
1
0
0
2.5
5
EQ. VOLUME GAIN [CC/100 GM POLYMER]
24.5°C
35.0°C
45.0°C

Fig. 21

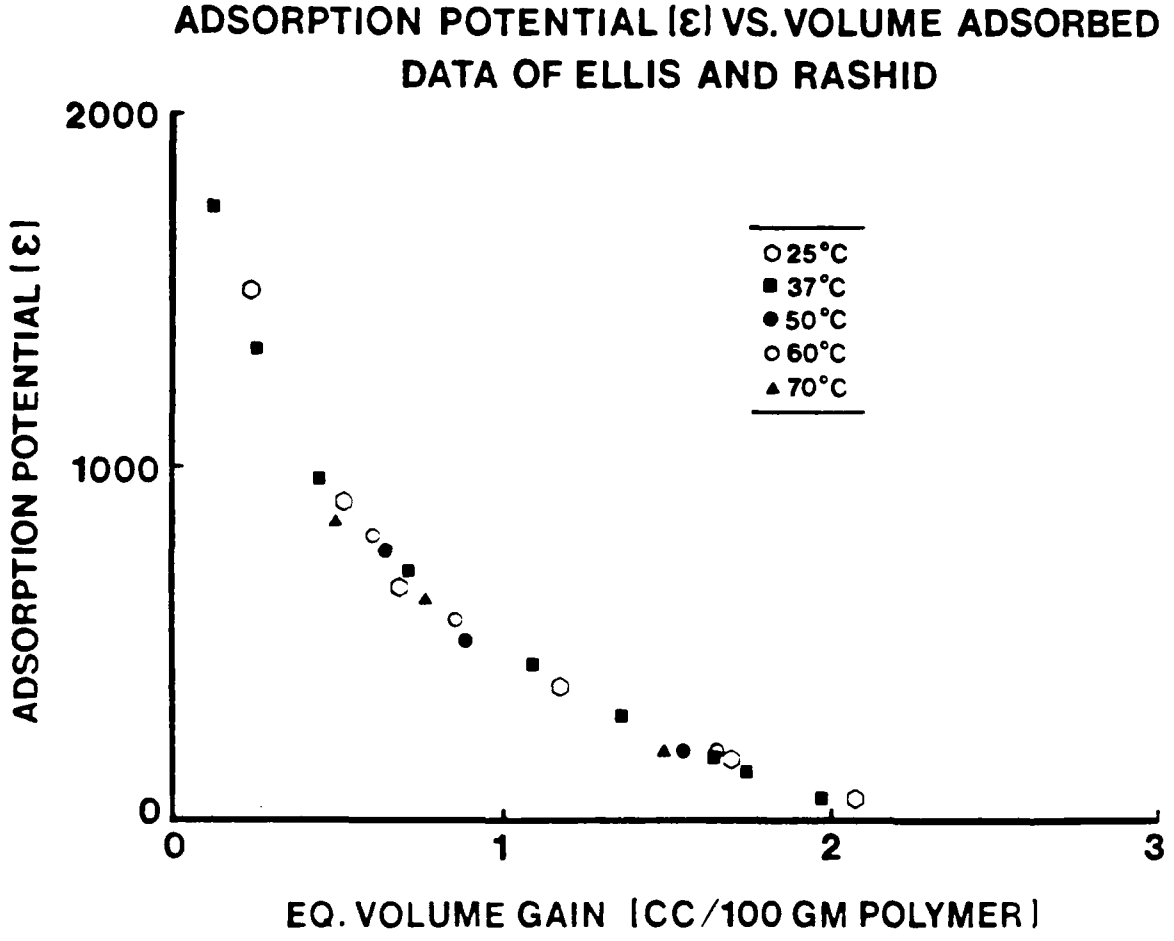
ADSORPTION POTENTIAL (ε) VS. VOLUME ADSORBED
DATA OF ELLIS AND RASHID
ADSORPTION POTENTIAL (ε)
2000
1000
0
0
1
2
3
EQ. VOLUME GAIN (CC/100 GM POLYMER)
25°C
37°C
50°C
60°C
70°C

Fig. 22

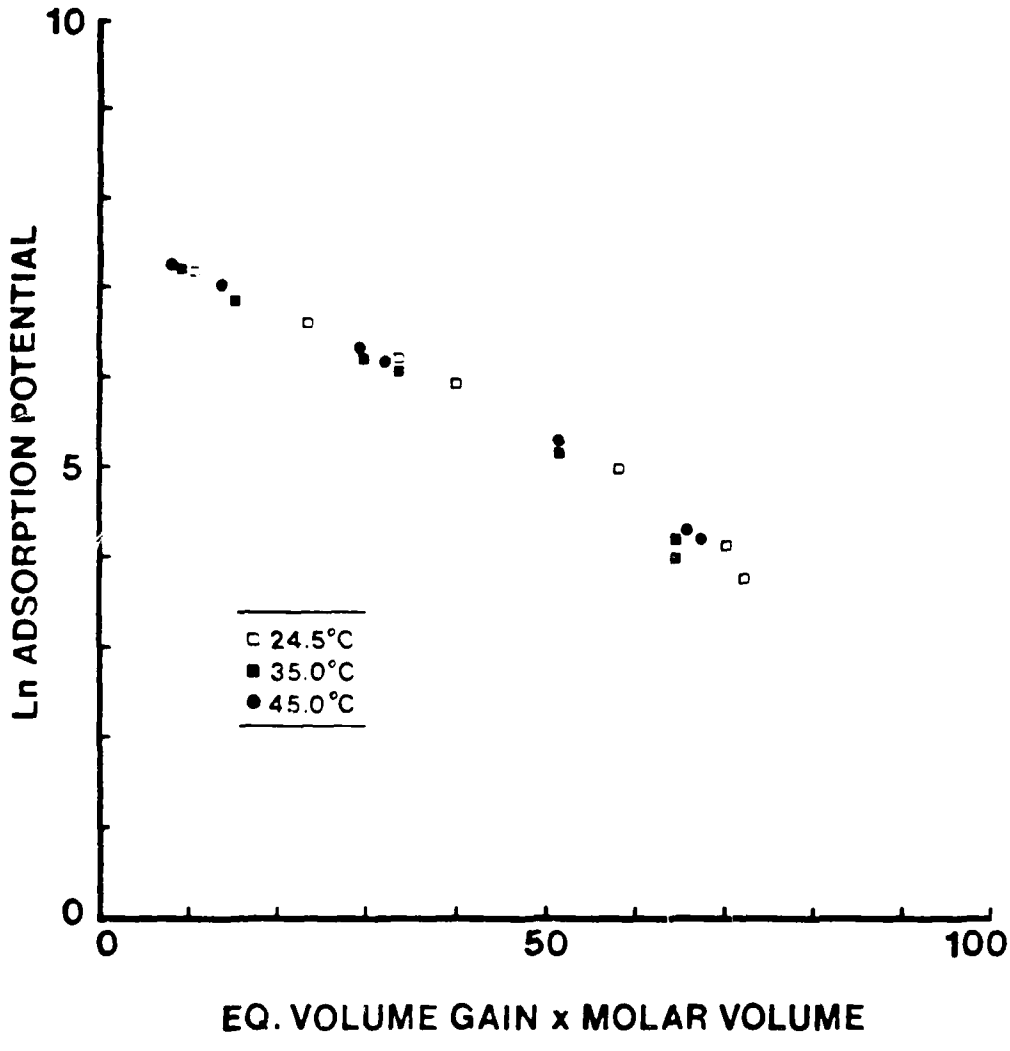
Ln ADSORPTION POTENTIAL
VS. VOLUME ADSORBED x MOLAR VOLUME
XD/TMAB [195°C/24 HR]
10
5
0
Ln ADSORPTION POTENTIAL
0
50
100
EQ. VOLUME GAIN x MOLAR VOLUME
24.5°C
35.0°C
45.0°C

Fig. 23

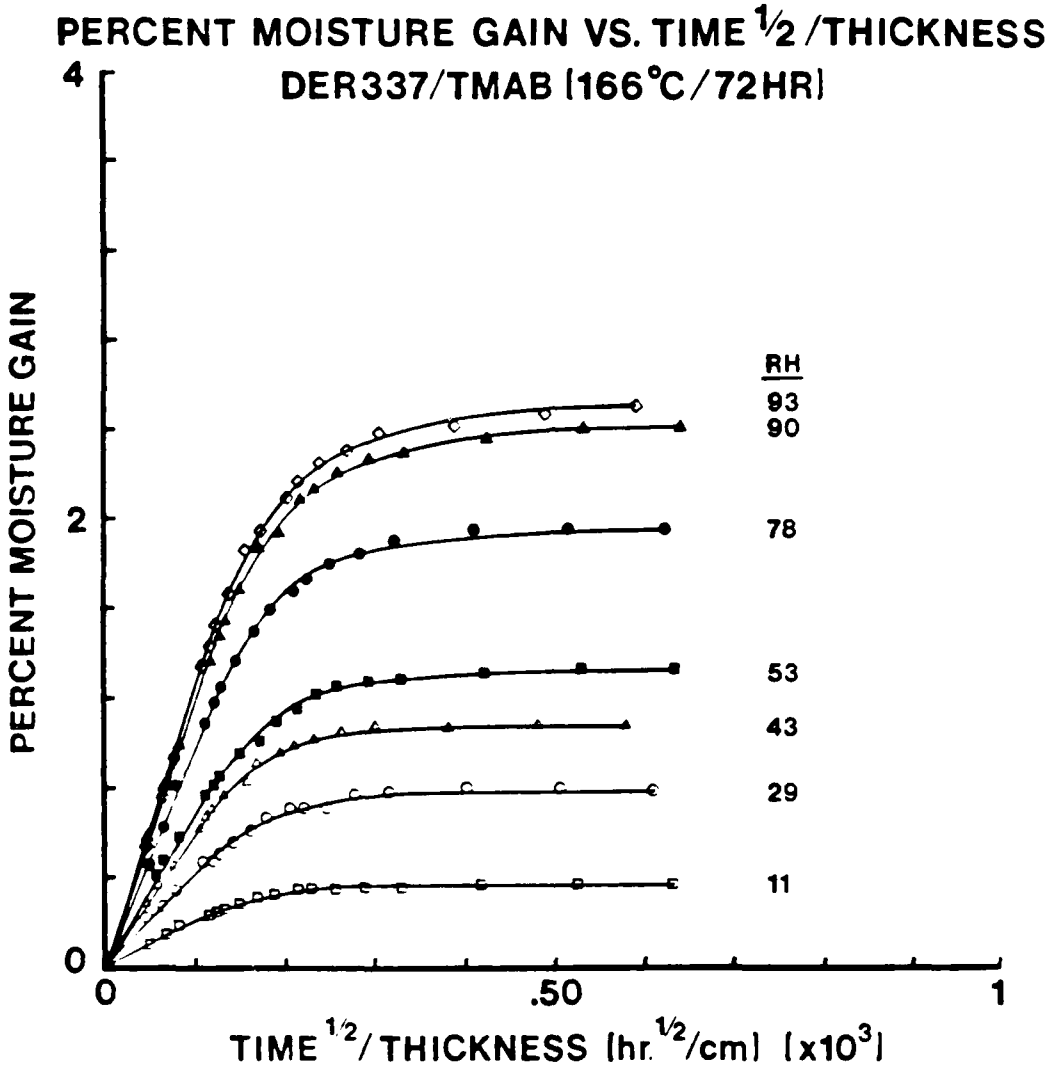
PERCENT MOISTURE GAIN VS. TIME 1/2 /THICKNESS
DER337/TMAB [166°C/72HR]
PERCENT MOISTURE GAIN
4
2
0
0
.50
1
TIME 1/2 / THICKNESS [hr. 1/2 /cm] [x10 3]
RH
93
90
78
53
43
29
11

Fig. 24a

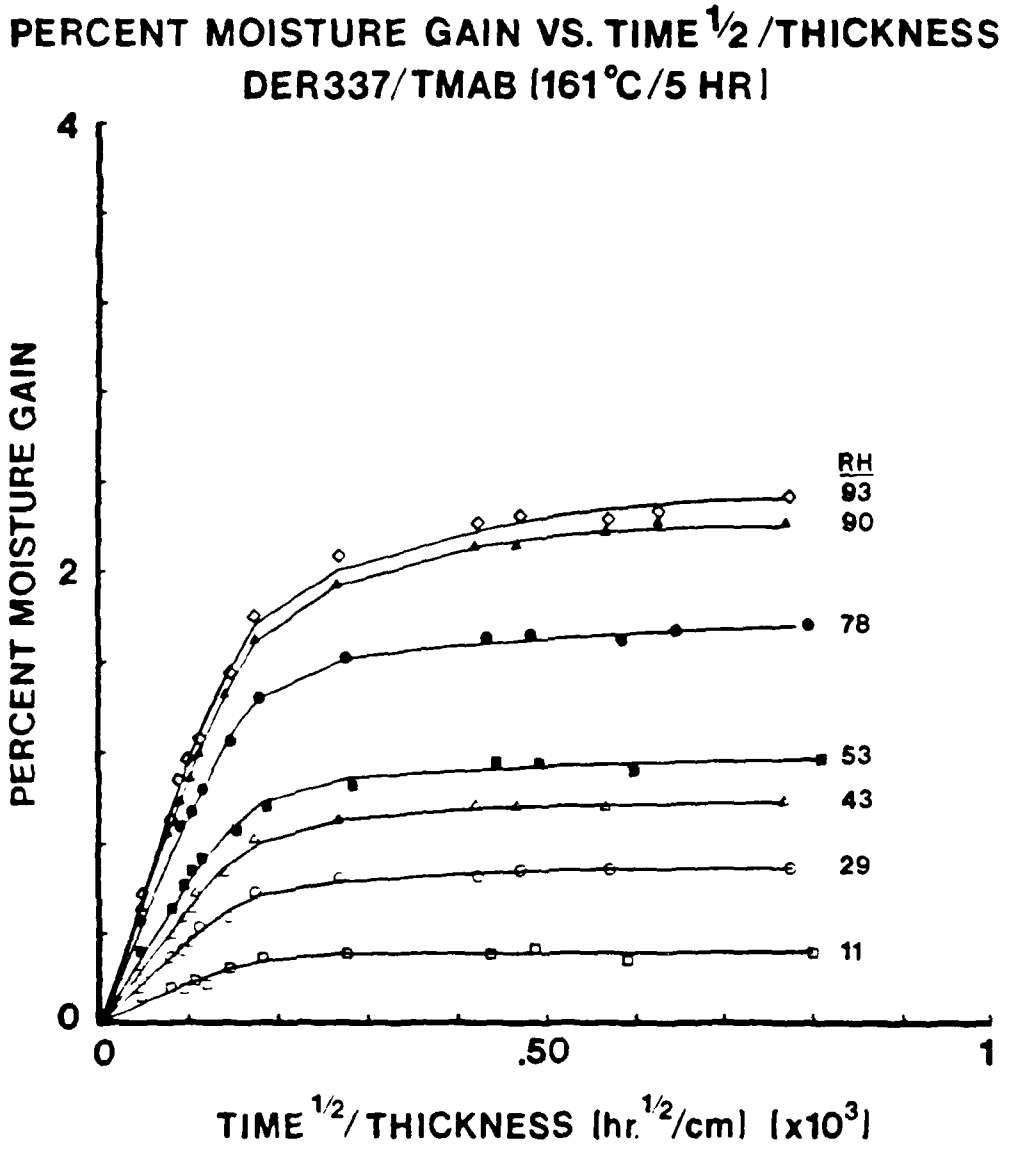
PERCENT MOISTURE GAIN VS. TIME 1/2 /THICKNESS
DER337/TMAB (161°C/5 HR)
PERCENT MOISTURE GAIN
4
2
0
0
.50
1
TIME 1/2/ THICKNESS (hr.1/2/cm) (x10³)
RH
93
90
78
53
43
29
11

Fig. 24b

PERCENT MOISTURE GAIN VS. TIME $^{1}/_{2}$ /THICKNESS
XD/TMAB (195°C/24 HR)

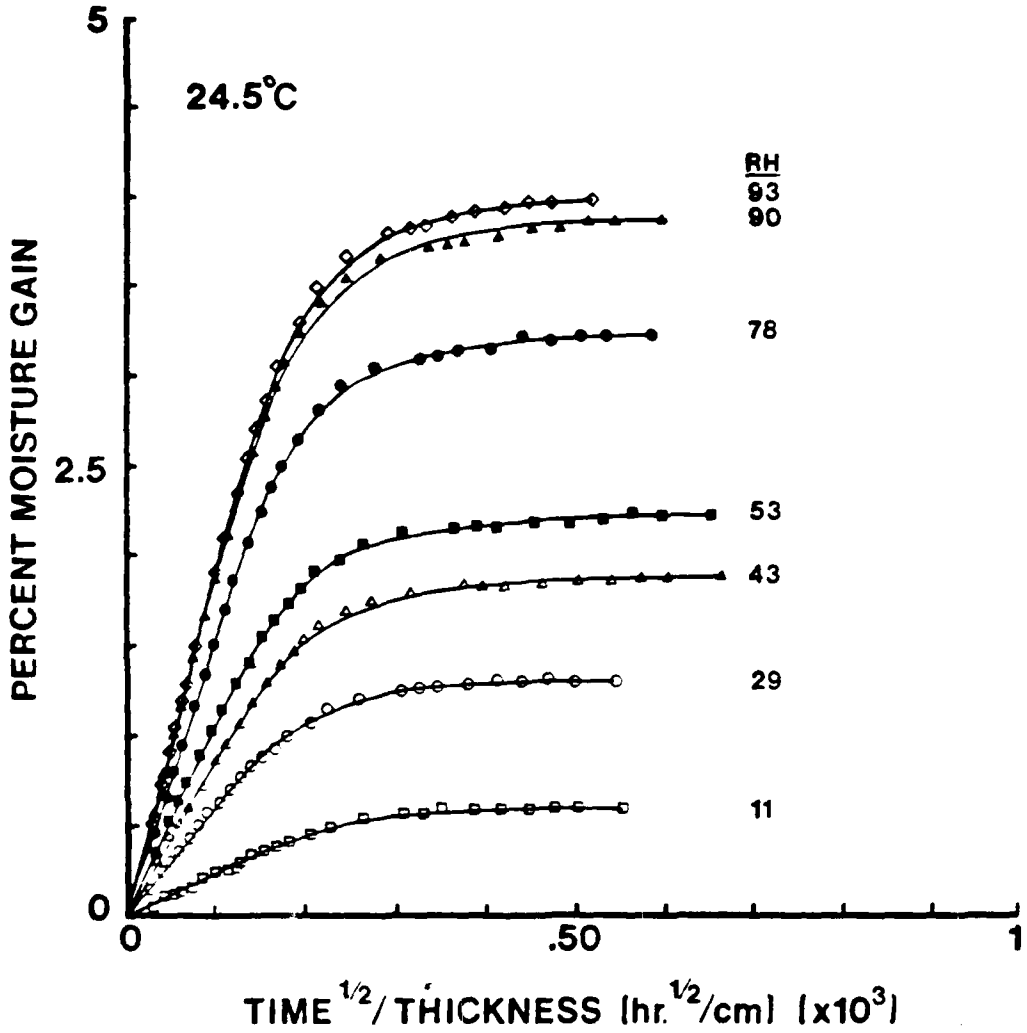

Fig. 24c

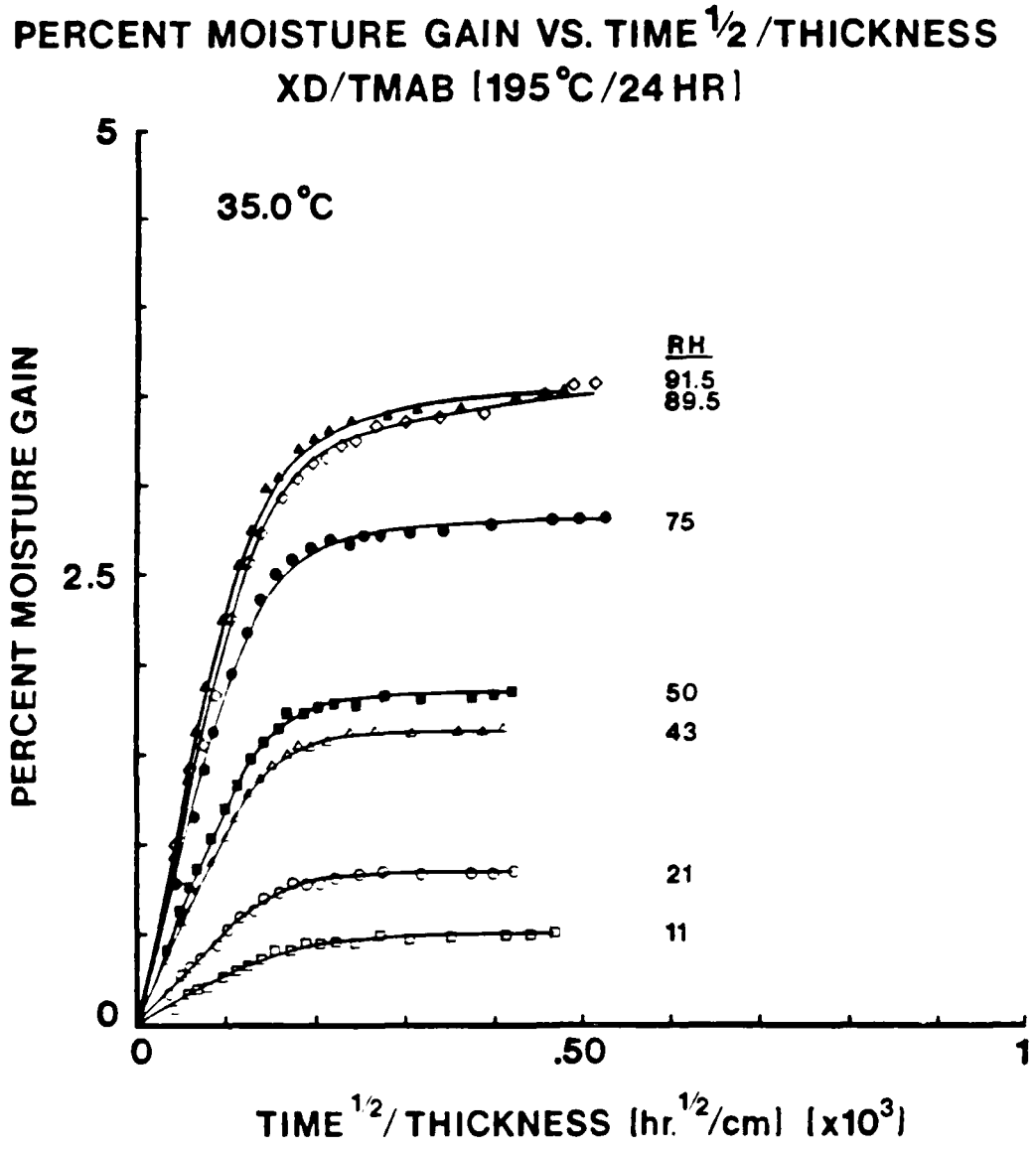
PERCENT MOISTURE GAIN VS. TIME 1/2 /THICKNESS
XD/TMAB [195°C/24 HR]
35.0°C
PERCENT MOISTURE GAIN
5
2.5
0
RH
91.5
89.5
75
50
43
21
11
0
.50
1
TIME 1/2 / THICKNESS [hr. 1/2/cm] [x10³]

Fig. 24d

EFFECT OF POST-CURE ON GLASSY-STATE PROPERTIES OF THERMOSETS

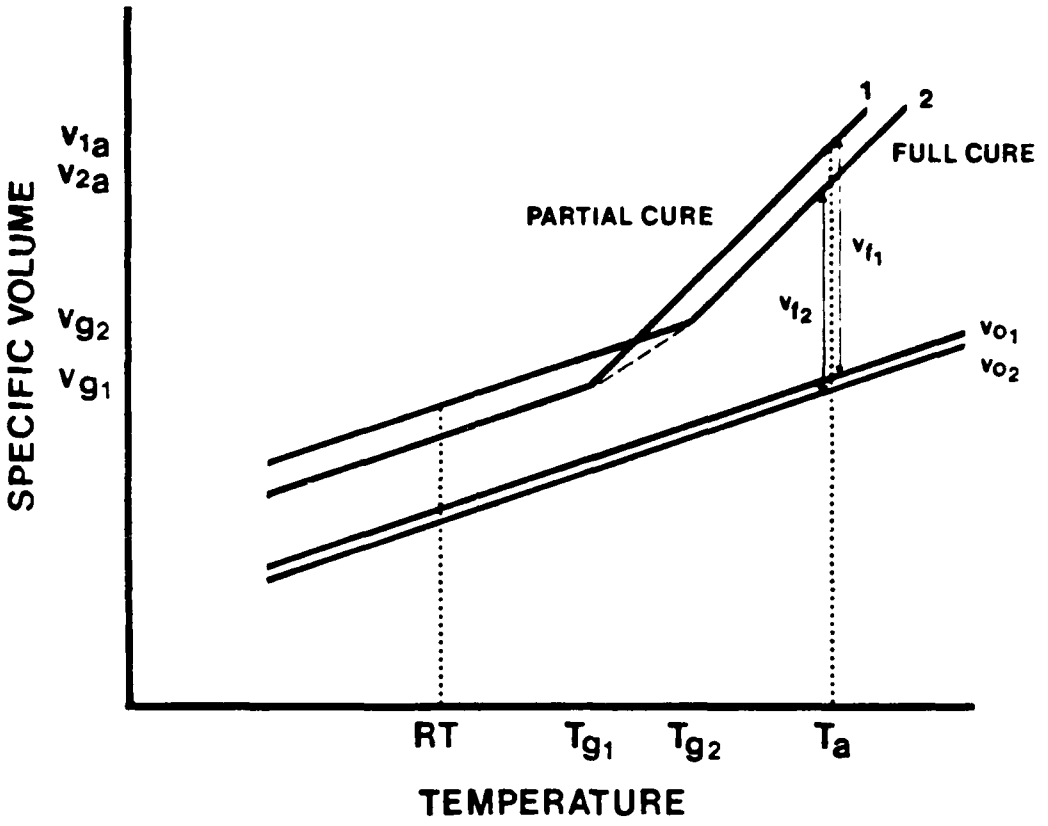

Fig. 25

DL/413/83/01
GEN/413-2

TECHNICAL REPORT DISTRIBUTION LIST, GEN

	No. Copies
Office of Naval Research Attn: Code 413 800 N. Quincy Street Arlington, Virginia 22217	2
Dr. Bernard Douda Naval Weapons Support Center Code 5042 Crane, Indiana 47522	1
Commander, Naval Air Systems Command Attn: Code 310C (H. Rosenwasser) Washington, D.C. 20360	1
Naval Civil Engineering Laboratory Attn: Dr. R. W. Drisko Port Hueneme, California 93401	1
Defense Technical Information Center Building 5, Cameron Station Alexandria, Virginia 22314	12
DTNSRDC Attn: Dr. G. Bosmajian Applied Chemistry Division Annapolis, Maryland 21401	1
Dr. William Tolles Superintendent Chemistry Division, Code 6100 Naval Research Laboratory Washington, D.C. 20375	1
Dr. David Young Code 334 NORDA NSTL, Mississippi 39529	1
Naval Weapons Center Attn: Dr. A. B. Amster Chemistry Division China Lake, California 93555	1
Scientific Advisor Commandant of the Marine Corps Code RD-1 Washington, D.C. 20380	1
U.S. Army Research Office Attn: CRD-AA-IP P.O. Box 12211 Research Triangle Park, NC 27709	1
Mr. John Boyle Materials Branch Naval Ship Engineering Center Philadelphia, Pennsylvania 19112	1
Naval Ocean Systems Center Attn: Dr. S. Yamamoto Marine Sciences Division San Diego, California 91232	1

END

DTIC

7-86